DISSERTATION

# Fundamental Study of Coronary Angioscopy using Spherical Ultrasonic Motor

Tokyo University of Agriculture and Technology,

Graduate School of Engineering,

Department of Mechanical Systems Engineering

**Fulin Wang**

February 2019

# Abstract

In this study, a new coronary angioscopy with a miniature motor used to adjust the direction of a coronary angioscopic camera is aimed to develop. The coronary angioscopy is very small in diameter, so it is difficult to mount a general actuator. Therefore, the camera cannot be driven in any direction. Therefore, there is a problem that the lesion in the blood vessel can be contained in the center of the image and cannot be observed from the front. As a solution to this problem, it can be mentioned a method of post processing to an image taken by using a wide angle lens with wide field of view and a method of moving the tip from the outside by using a wire. However, there is a problem that the time lag occurs as image processing is necessary in the former method, and there is a problem that there is no space for bending the tip in a narrowly curved blood vessel in the latter method.

The lesion on the inner wall surface of the blood vessel can be contained in the center of the image by driving a miniature motor in a new coronary angioscopy. Spherical ultrasonic motor not affected by magnetic fields is used in the miniature motor. The characteristic of spherical ultrasonic motor is that one motor has multi degree of freedom in rotational direction. In the previous study, three stators used in a flat plate type ultrasonic motor with one degree of freedom of rotation are used for one spherical rotor, and a spherical ultrasonic motor capable of three degree of freedom drive of rotation has been developed by synthesizing rotational direction components generated from each stator. Furthermore, a miniature spherical ultrasonic motor equipped with a camera has been developed as an actuator mounted on a hard mirror used for surgical angioscopy. However, the finished miniature spherical ultrasonic motor has a stator of 14 mm diameter, and this size is large for the coronary angioscopy. Therefore, it is difficult to realize a smaller size when a stator similar to the conventional ultrasonic motor is used.

Based on the above problems, a miniature spherical ultrasonic motor using wire stators suitable for miniaturization have is being developed. A wire is used as a stator to realize miniaturization of a motor, so it is called miniature spherical ultrasonic motor using wire stators. The miniature spherical ultrasonic motor using wire stators is based on the basic structure of the conventional spherical ultrasonic motor, and two degree of freedom drive is possible. Further miniaturization is expected by using the wire stator with the waveguide that the stator part has a simple structure. Miniaturization to the size that can be mounted on the coronary angioscopy is expected to solve the problem in the above described coronary angioscopy. For the miniature spherical ultrasonic motor using wire stators developed for that purpose, acquisition of basic characteristics and establishment of control method are aimed. Moreover, the waveguide and the holding method mounted on the coronary angioscopy are also discussed.

# Contents

# Chapter 1. Introduction

## 1.1. Research background

The ischemic heart disease caused by arteriosclerosis occupies higher cause of death in the world, and it is one of the three major causes of death in Japan. The annual transition of crude mortality rate by the major cause of death to 100,000 population is shown in Fig. 1.1 [1]. The number of deaths due to heart disease decreased from 1993 to 1995, since the death certificate based on the International Classification of Diseases: ICD-10 was revised in 1995, and it was reflected as statistical material since 1994. Arteriosclerosis is caused by the hardening of blood vessels due to aging and stenosis of the blood vessel lumen due to accumulation of plaque.

Coronary angiography (CAG) and intravascular ultrasound (IVUS) [2-3] have been used for the examination and observation of the blood vessel lumen. Coronary angioscopy [4-9] technically improved has been used in the medical field in the 1980s. For comparison with coronary angiography and intravascular ultrasound [10-14], it can be indicated that coronary angioscopy is effective. As the advantages of the coronary angioscopy, there are three dimensional, full color, and high resolution of the luminal surface of a blood vessel. As the disadvantage of the coronary angioscopy, it can be mentioned that it is difficult to block the blood flow at the time of observation and observe the inside of the blood vessel wall. In addition, it is difficult to photograph the lesion of the wall in the center of the image in the existing coronary angioscopic camera in the observation of the blood vessel lumen. In order to carry out the correct diagnosis, it can be desired to photograph the lesion in the center of the image.

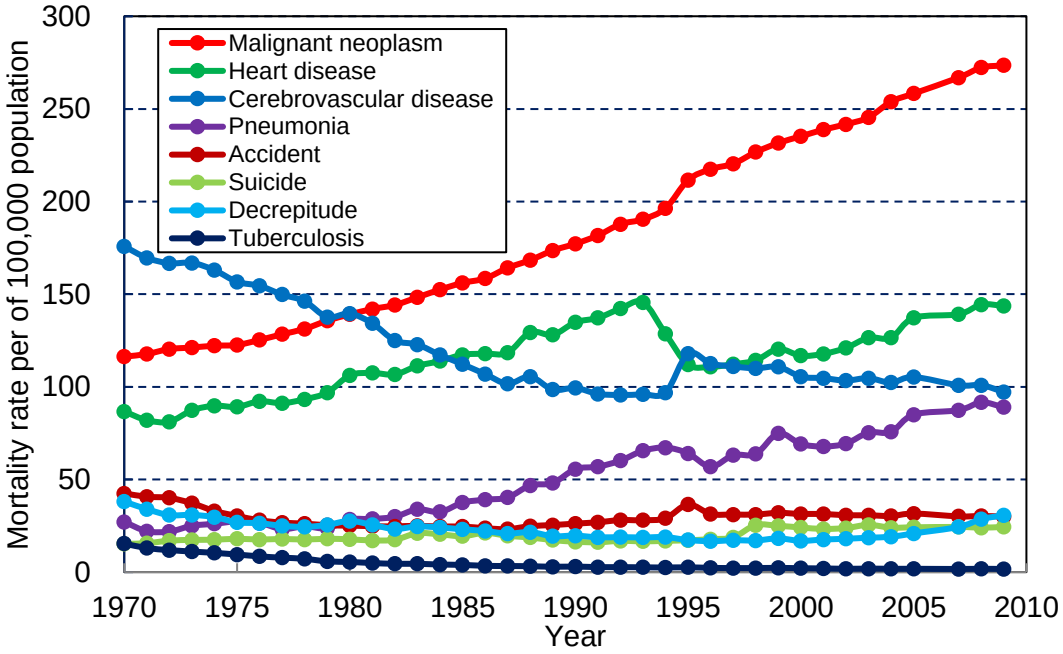


Fig. 1.1 Major cause-specific crude mortality.

## 1.2. Current status of intravascular examination

### 1.2.1. Coronary angiography (CAG)

The CAG (coronary angiography) is an examination method for diagnosing lesions using X-ray and X-ray contrast substance. The state of blood vessel and blood flow is continuously taken by using X-ray absorption difference. The catheter is inserted from the artery of the thigh root or the arm and the contrast medium is injected into the blood vessel to be examined, and the diagnosis is carried out by X-ray photography.

There is an advantage that not only the shape of the blood vessel but also the state of the blood flow can be observed, but it is difficult to grasp the morphology of the stenotic part in order to diagnose the stenosis degree of blood vessel. In addition, there are problems that the exacerbation of renal function and the transition to renal failure are feared in the case in which the renal function is lowered in the patient and there is also a case in which the allergic reaction to contrast media may be exhibited [15].

### 1.2.2. Intravascular ultrasound (IVUS) [16]

The IVUS (intravascular ultrasound) is an imaging examination method in real time to visualize blood vessel cross section from the inside blood vessel using ultrasound. A catheter with an ultrasonic probe mounted at the tip is inserted into the blood vessel, and the ultrasonic wave emitted from an ultrasonic probe is mechanically or electronically radial scanned. In addition to the position and stenosis degree of the stenotic part, the hardness of the blood vessel and the state outside blood vessel can be known.

The IVUS has a mechanical scanning type in which the scanning is carried out from an external motor by rotating an ultrasonic probe through a torque wire and has an electronic scanning type in which the scanning is carried out by electrically and continuously exciting multiple ultrasonic vibrators arranged around the catheter axis. In the case of the mechanical scanning type IVUS, there is a problem that the image becomes disordered and the rotational unevenness occurs due to the complexity of the mechanism and the bending of the torque wire. In the case of the electronic scanning type IVUS, the image quality is deteriorated due to the small size of the vibrator as the probe.

### 1.2.3. Optical coherence tomography (OCT) [17-18]

OCT (Optical Coherence Tomography) is an examination method for observing by obtaining an accurate tomogram of a tissue using an optical interferometer. The near infrared light is radiated from the catheter probe. First, the near infrared light emitted from the light source is divided into two, one is illuminated to the object as the measurement light, and the other is illuminated to the reference mirror. Next, an interference phenomenon occurs by polymerizing two light reflected from each other, and the two dimensional tomogram is constructed by measuring the intensity of light reflection of the object and time delay.

The resolution of OCT is approximately 10 $\mu$m to 15 $\mu$m, which has approximately 10 times higher resolution than IVUS. Furthermore, IVUS is superior to the evaluation of thrombus and calcification which is difficult to observe. However, there is the irregular reflection and damping of the near infrared ray due to the erythrocyte in the observation, so blood exclusion in the coronary artery is necessary. In addition, it is inferior in the deep part reachability of the image, so there is a disadvantage that it is difficult to evaluate the whole image in the part where the vessel diameter is large.

### 1.2.4. Coronary angioscopy [19]

Coronary angioscopy is an examination method for direct observation of the lesion by inserting an angionscopic catheter into the blood vessel. The diameter of the angionscopic catheter is approximately 0.5 to 2 mm. The evaluation of obtaining the intravascular tomographic image is carried out in IVUS and OCT, and the evaluation of the luminal surface of a blood vessel is carried out in coronary angioscopy, but more detailed histopathological diagnosis is possible by comparison with other examination methods.

As shown in Fig. 1.2, the image is a three dimensional real color image, so the color tone of the plaque and thrombus and the fine morphology of the surface can be observed. Furthermore, it can be expected to be used for intravascular treatment under coronary angioscopy in the future. Laser ablation [20] and plaque extirpation [21] under coronary angioscopy have already been carried out. In addition, the mechanism of the coronary artery lesion which cannot be solved by the above examination method can be clarified. Up to now, the disease prediction of probability and epidemiology can be carried out more accurately, and it is very useful from the viewpoint of early diagnosis.

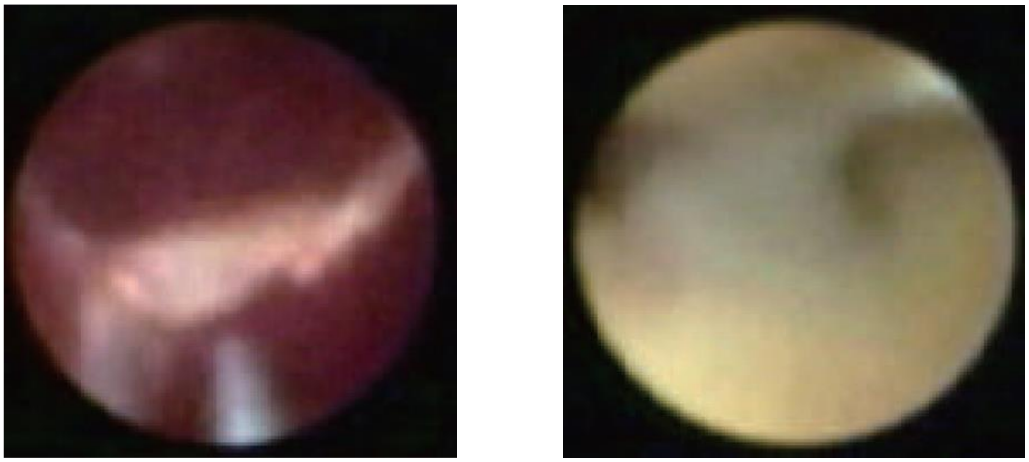

(a) Red thrombus (b) White thrombus

Fig. 1.2 Intravascular image.

## 1.3. Purpose of study

The coronary angioscopy is very small in diameter, so it is difficult to mount a general actuator. Therefore, the camera cannot be driven in any direction. Therefore, there is a problem that the lesion in the blood vessel can be contained in the center of the image and cannot be observed from the front. As a solution to this problem, it can be mentioned a method of post processing to an image taken by using a wide angle lens with wide field of view and a method of moving the tip from the outside by using a wire. However, there is a problem that the time lag occurs as image processing is necessary in the former method, and there is a problem that there is no space for bending the tip in a narrowly curved blood vessel in the latter method.

In this study, a new coronary angioscopy with a miniature motor used to adjust the direction of a coronary angioscopic camera is aimed to develop. The lesion on the inner wall surface of the blood vessel can be contained in the center of the image by driving a miniature motor in a new coronary angioscopy. Spherical ultrasonic motor not affected by magnetic fields is used in the miniature motor. The characteristic of spherical ultrasonic motor is that one motor has multi degree of freedom in rotational direction.

In the previous study [22], three stators used in a flat plate type ultrasonic motor [23] with one degree of freedom of rotation are used for one spherical rotor, and a spherical ultrasonic motor capable of three degree of freedom drive of rotation has been developed by synthesizing rotational direction components generated from each stator. Furthermore, a miniature spherical ultrasonic motor equipped with a camera has been developed as an actuator mounted on a hard mirror used for surgical angioscopy as shown in Fig. 1.3 [24]. However, the finished miniature spherical ultrasonic motor has a stator of 14 mm diameter, and this size is large for the coronary angioscopy. Therefore, it is difficult to realize a smaller size when a stator similar to the conventional ultrasonic motor is used.

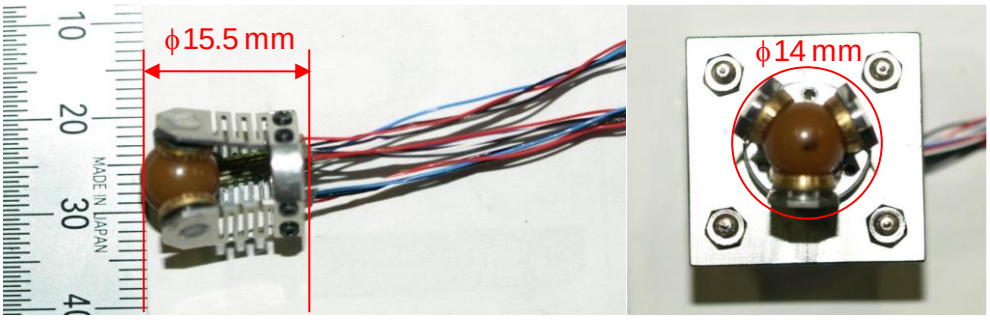


Fig. 1.3 Compact spherical ultrasonic motor.

Based on the above problems, a miniature spherical ultrasonic motor using wire stators suitable for miniaturization is being developed. A wire is used as a stator to realize miniaturization of a motor, so it is called miniature spherical ultrasonic motor using wire stators. The miniature spherical ultrasonic motor using wire stators is based on the basic structure of the conventional spherical ultrasonic motor, and two degree of freedom drive is possible. Further miniaturization is expected by using the wire stator with the waveguide that the stator part has a simple structure. Miniaturization to the size that can be mounted on the coronary angioscopy is expected to solve the problem in the above described coronary angioscopy. For the miniature spherical ultrasonic motor using wire stators developed for that purpose, acquisition of basic characteristics and establishment of control method are aimed. Moreover, the waveguide and the holding method mounted on the coronary angioscopy are also discussed. The added value of the new coronary angioscopy is that the lesion can be photographed in the center of the image at the observation of the blood vessel lumen. It can be expected that the lesion can be grasped more reliably than the current coronary angioscopy if the miniature spherical ultrasonic motor using wire stators is completed. A conceptual diagram of a miniature spherical ultrasonic motor mounted on a coronary angioscopy is shown in Fig. 1.4. The target size of the spherical rotor, which is the largest component, is 0.8 mm in diameter and is a feasible size. However, the size of the motor in this study is larger than the actual size in order to give priority to easiness of experiment. The diameter of the spherical rotor in the motor used is 15 mm. However, rotational driving of a spherical rotor with a diameter of 3 mm has been carried out in Toyama laboratory at the Tokyo University of Agriculture and Technology, but it can be known that the influence on the result due to the difference in the motor size is small. On the other hand, in the miniature motor, the rotational speed and the rotational direction can be controlled, and the position control cannot be carried out. The operator manually operates regarding the movement in the depth direction, but the rotational speed and the rotational direction are electrically carried out. The application is to photograph a static image or a video of a lesion by a camera, but it cannot be thought that the lesion is photographed at pinpoint. It is sufficient to be able to photograph while rotating in the direction to the inner wall of the blood vessel. In addition, it is a future work that it is difficult to control the position of a spherical ultrasonic motor with a plurality of stators and it is not limited to the wire stator type. In addition, the rotational speed required for a miniature motor is approximately 180 rpm. The rotational speed slower than the camera frame rate (30 fps) is sufficient since the application is to photograph a static image or a video of a lesion by a camera.

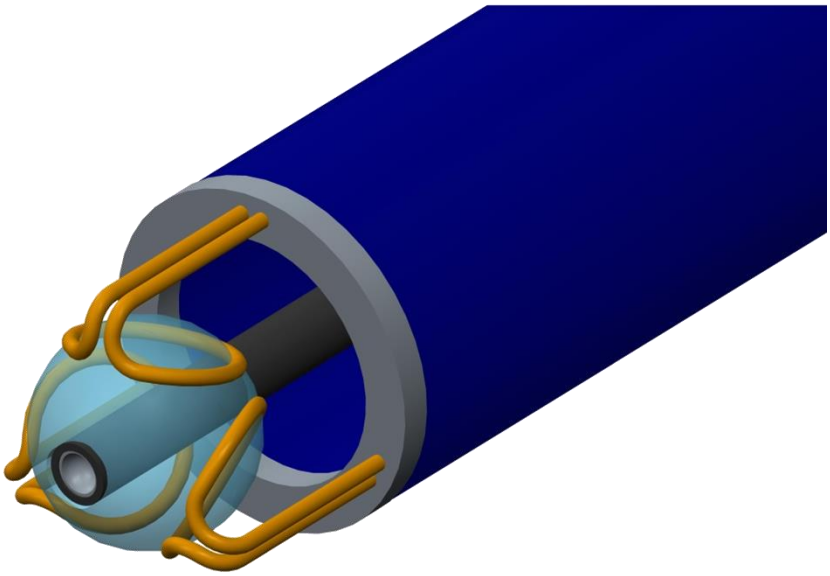

Fig. 1.4 Concept of new angioscopy.

## 1.4. Composition of this doctoral dissertation

This doctoral dissertation consists of seven chapters. The outline of each chapter is described below.

In Chapter 1, the method of intravascular examination actually being practiced is briefly described, and the problems of coronary angioscopy and the purpose of this study are shown.

In Chapter 2, driving principle of a miniature spherical ultrasonic motor using wire stators is described. In addition, driving principle of the traveling wave type ultrasonic motor is described, and an ultrasonic motor with coil stator driven by a similar driving principle is introduced. Finally, the driving parameters are discussed.

In Chapter 3, the experiments of a miniature spherical ultrasonic motor using wire stators using a spherical rotor of 15mm diameter. As basic characteristics, the relationship between the pressing force and the rotational speed and the starting torque on the one axis is investigated, and the experimental results are described.

In Chapter 4, the control method of a miniature spherical ultrasonic motor using wire stators is discussed. A PWM control method to control the rotational direction of an ultrasonic motor is proposed, and the method and experimental results are described.

In Chapter 5, the transient response analysis by the finite element method is performed for a 2 m waveguide by assuming the introduction to a coronary angioscopy, and the decreasing rate of input amplitude due to the influence of waveguide is discussed.

In Chapter 6, the transient response analysis by the finite element method is performed for the model of wire stator with support structure, and the influence of damping due to structure and vibration direction is described. The transient response analysis of the proposed appropriate support structure is performed, and damping of input vibration is discussed.

In Chapter 7, the results of this study are described.

# Chapter 2. Spherical ultrasonic motor using wire stators

## 2.1. Ultrasonic motor

Ultrasonic motor [25-32] is an actuator driven by mechanical vibration of ultrasonic fields (the acoustic wave and the vibration of an object of frequency above 20 kHz). Therefore, the sound generated by the motor also becomes an ultrasonic field, and it is excellent in silence as it exceeds human audible area (20 Hz to 20 kHz). According to the driving principle of the ultrasonic motor, it can be driven by the contact between the stator vibration surface and the rotor part, so it is possible to realize the rotational motion by a simple mechanism. Therefore, it is suitable for miniaturization and lightening. In addition, by the mechanism which generates the mechanical vibration to the stator, it can be classified into wedge type, traveling wave type, complex vibration type [33]. The spherical ultrasonic motor using wire stators being developed in the Toyama laboratory at the Tokyo University of Agriculture and Technology applies the principle of a spherical ultrasonic motor and an ultrasonic motor with coil stator which are one type of traveling wave type ultrasonic motors. Here, the driving principle and features of traveling wave type ultrasonic motor, spherical ultrasonic motor and ultrasonic motor with coil stator are explained.

### 2.1.1. Traveling wave type ultrasonic motor

The traveling wave type ultrasonic motor is an actuator which uses the mechanical vibration in the ultrasonic fields as the driving source. This ultrasonic wave means the acoustic wave and the vibration of an object of frequency above 20 kHz. This motor performs elliptical motion of the mass point on the surface of an elastic body by traveling wave of ultrasonic vibration, and the driving force is obtained through friction. The traveling wave shown here is the wave which apparently propagates in the certain direction while maintaining the wave state such as ripples on the water surface or light can be mentioned. A bending traveling wave propagating in an elastic body is shown in Fig. 2.1. By pressing the moving body from above the elastic body with a certain preload, driving force is obtained as the elliptical motion is transmitted to the moving body by friction.

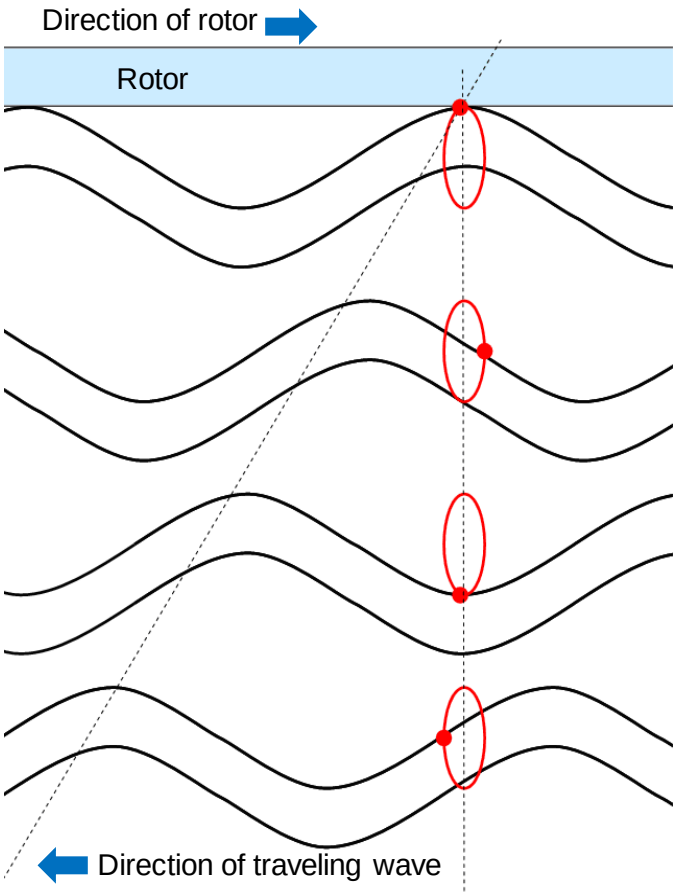


Fig. 2.1 Propagation of wave.

The motion of an elastic body surface caused by traveling waves can be considered using a partial model of the elastic body shown in Fig 2.2. Here, the neutral axis in the state without deflection is defined as $x$ axis, and the direction of the thickness in the positive direction of the contact surface with the moving object is defined as $y$ axis. Furthermore, it can be assumed that the point on the neutral axis of the elastic body can hardly move in $x$ direction, and the cross section perpendicular to the neutral axis in the state without deflection is always perpendicular to the neutral axis. Here, the traveling wave can be expressed by the following equation (2.1). However, $A$ is the amplitude, and $x$ is the function of the position, and $T$ is the function of the time $t$ :

$$y = A \cdot \sin\left(X(x) + T(t)\right) \tag{2.1}$$

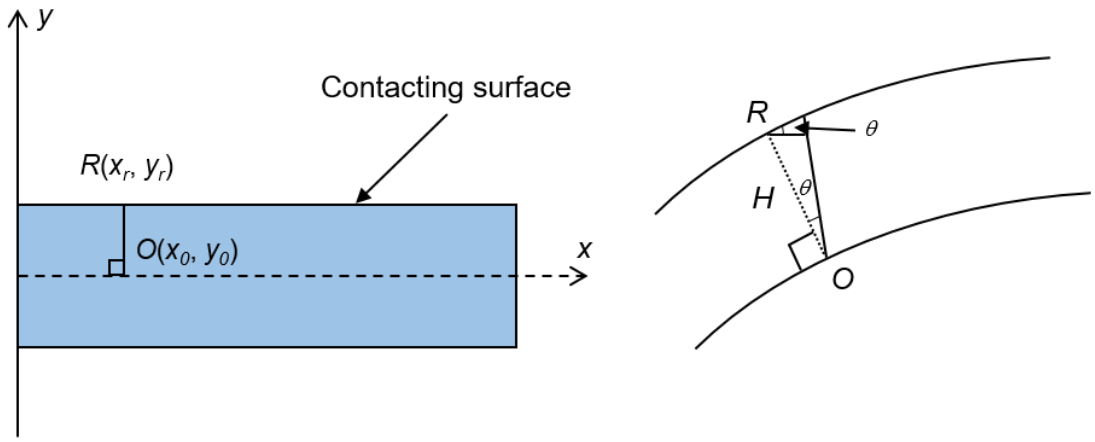


(a) Definition of coordinates (b) Deflection angle

Fig. 2.2 Model of elastic body.

The point M( $x_m$ , $y_m$ ) on the neutral axis and the point R( $x_r$ , $y_r$ ) on the contact surface of the moving object can be considered. First, the motion of the point M is represented by the equation (2.1) where the function $X(x)$ of the position $x$ and the function $T(t)$ of the time $t$ take the following initial values:

$$\begin{cases} x = 0 \rightarrow X(x) = 0 \\ t = 0 \rightarrow T(t) = 0 \end{cases}$$

Thus, the motion of point M is as follows from equation (2.1):

$$y_m = A \cdot \sin\left( \frac{2\pi}{\lambda} x_m + \omega t \right) \tag{2.2}$$

Where $A$ is the amplitude, and $\lambda$ is the wavelength, and $\omega$ is the angular frequencies of the wave.

Next, the point R can be considered. In Fig. 2.2(b), the deflection angle $\theta$ is:

$$\theta = \left[ \frac{\partial y_m}{\partial x} \right]_{x=x_m} = A \cdot \frac{2\pi}{\lambda} \cdot \cos\left( \frac{2\pi}{\lambda} x_m + \varpi t \right) \tag{2.3}$$

In addition, $x_r$ using the distance H and $\theta$ of the point O and the point R can be expressed as follows:

$$x_r = x_m - H \cdot \sin\theta \cong x_m - H\theta \tag{2.4}$$

Similarly, $y_r$ can be expressed as follows:

$$y_r = y_m + H \cdot \cos\theta \cong y_m + H\theta \tag{2.5}$$

Therefore, from equations (2.2) to (2.5), $x_r$ and $y_r$ are:

$$x_r = x_m - H \cdot A \cdot \frac{2\pi}{\lambda} \cdot \cos\left( \frac{2\pi}{\lambda} x_m + \omega t \right) \tag{2.6}$$

$$y_r = A \cdot \sin\left( \frac{2\pi}{\lambda} x_m + \varpi t \right) + H \tag{2.7}$$

Next, the displacement of the point R can be considered. The displacement of $x_r$ and $y_r$ are respectively $X_r$ and $Y_r$. For simplification, $(2\pi/\lambda \cdot x_m + \omega t)$ is the function $U$ of the time, and by replacing $H \cdot 2\pi/\lambda = N$, $X_r$ and $Y_r$ are as follows:

$$X_r = x_r - x_m = -N \cdot A \cdot \cos U \tag{2.8}$$

$$Y_r = y_r - H = A \cdot \sin U \tag{2.9}$$

$U$ is eliminated from the equations (2.8) and (2.9), and the following equation is:

$$\frac{{X_r}^2}{(-N \cdot A)^2} + \frac{{Y_r}^2}{A^2} = 1 \tag{2.10}$$

The equation (2.10) indicates that the point R has elliptical motion of the lateral amplitude $A \cdot H \cdot 2\pi/\lambda$ and the vertical amplitude $A$. Thus, this elliptical motion is opposite to the traveling direction of the traveling wave, and it can be seen that the moving object moves in the opposite direction to the direction of the traveling wave.

### 2.1.2. Spherical ultrasonic motor

The spherical ultrasonic motor uses the driving principle of traveling wave type ultrasonic motor. In this section, first, with respect to the driving principle of a traveling wave type ultrasonic motor using annular stator and rotor, electrostrictive phenomenon of piezoelectric elements is converted into mechanical energy, and the movement of the stator surface transmitting to the rotor is theoretically expanded in Mathematics. Next, driving principle and features of a spherical ultrasonic motor are described.

The general structure of a traveling wave type ultrasonic motor is composed of an annular stator with piezoelectric elements pressed against an elastic body with cut comb teeth and a rotor as a moving object. The schematic diagram is shown in Fig. 2.3. By applying AC voltage in the ultrasonic fields to the piezoelectric elements, traveling wave propagating in a vibration medium on a stator surface is generated due to microvibration using electrostrictive phenomenon of the piezoelectric elements. This elliptical motion is transmitted to the rotor by friction. This type of motor has less abrasion compared with other ultrasonic motors since the collision operation between the rotor and the stator is continuous, so switching between forward rotation and reverse rotation can be performed by changing the traveling direction of the traveling wave. In addition, the pressure between the rotor and the stator are always pressurized, and the force acting between the rotor and the stator is constant when the rotor is stationary or low rotation. Therefore, there is the advantage that it has a holding force without a brake mechanism in a stationary state without the power supply and a large torque can be output at low rotation.

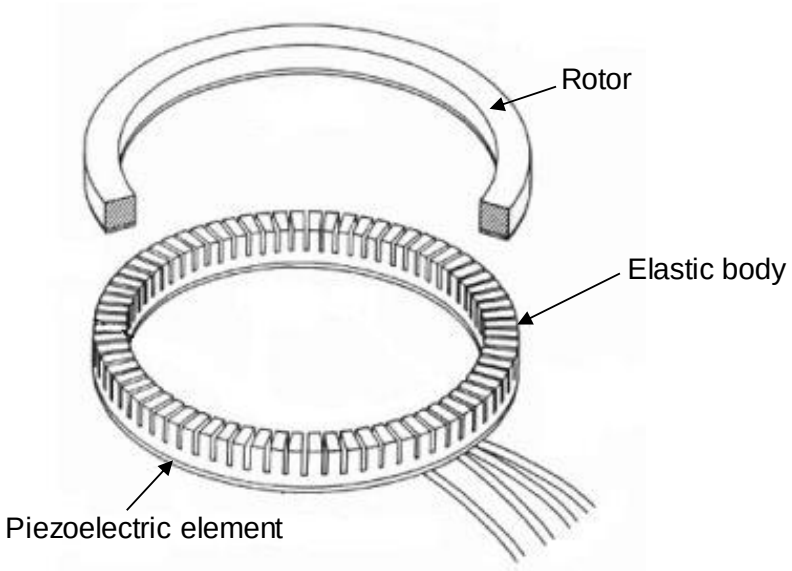


Fig. 2.3 Schematic diagram of ultrasonic motor.

Traveling wave type ultrasonic motor is driven by generating traveling wave in the circumferential direction on the stator surface. Most of the traveling wave type ultrasonic motors in practical use are annular, and a traveling wave having an integral number of wavelengths of the circumferential length is generated in the circumferential direction. The traveling wave is a wave traveling in the vibration medium, in contrast, the standing wave is a wave which can hardly change the positions of the wave belly and the wave band. The traveling wave is obtained by synthesizing two standing waves which are positionally and temporally shifted on the elastic body. The followings are mathematically expressed.

The positional vibration waveform of the standing wave with the temporal vibration amplitude $A$ are expressed by sine function, and the temporal vibration waveform is expressed by the cos function, and the standing wave can be expressed as follows:

$$y_1 = A \cdot \sin(\theta) \cdot \cos(T) \tag{2.11}$$

Where $\theta$ is the function of the position, $T$ is the function of the time. This standing wave and the standing wave of π/2 phase difference in the position and time can be expressed as follows:

$$y_2 = A \cdot \cos(\theta) \cdot \sin(T) \tag{2.12}$$

Two standing waves expressed by the equations (2.11) and (2.12) are synthesized and the following equation is expressed by the addition theorem of the trigonometric function:

$$y = y_1 + y_2 = A \cdot \sin(\theta + T) \tag{2.13}$$

In addition, where constant $C$ given as an initialization phase to generalize and the equation (2.13) can be expressed as follows:

$$y = y_1 + y_2 = A \cdot \sin(\theta + T + C) \tag{2.14}$$

The wave expressed by equation (2.14) is a wave traveling at a constant speed without

distorting the waveform. That is, the traveling wave is shown.

Next, the state of the generation of traveling wave is shown for the vibrator used in the spherical ultrasonic motor. The vibrator is shown in Fig 2.4. The vibrator has piezoelectric elements attached to an annular elastic body with comb shape notch and has an electrode mounted. The material of the elastic material is SUS403 which is a nonmagnetic material, and there is also the lining material coated with the fluorine resin when the nickel plating have be applied on the surface. This is to make the friction coefficient between the rotor and the vibrator good from 0.1 to 0.2 [34].

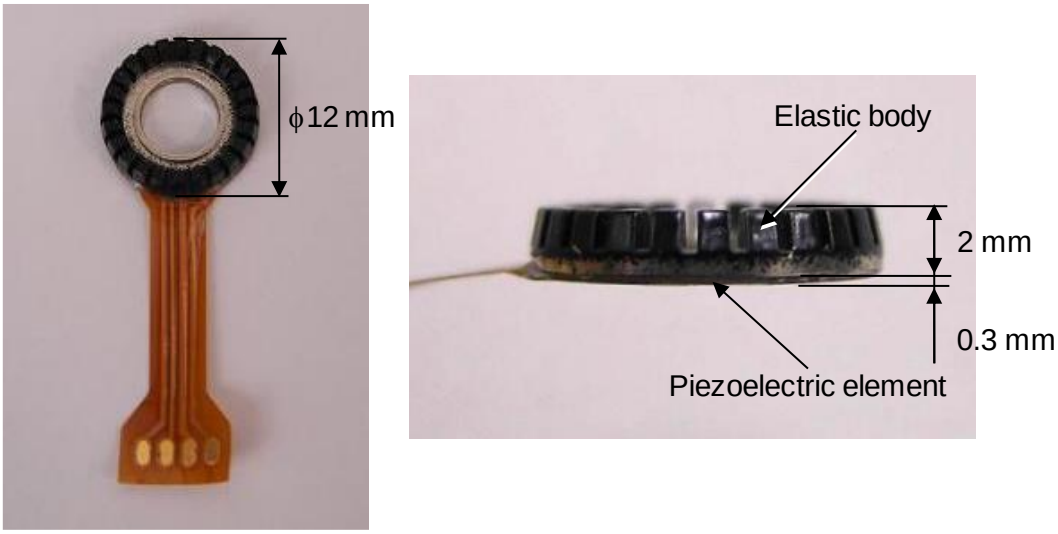


Fig. 2.4 Appearance of a vibrator.

In addition, the configuration diagram of the piezoelectric elements and electrodes is shown in Fig 2.5. The piezoelectric elements are polarized alternately plus and minus. There are four types of electrodes: phase A, phase B, GND and phase FB (Feed Back). Phase A and phase B are connected respectively to four left and right piezoelectric elements, and vibration is generated by applying voltage. GND is connected to an elastic body. Phase FB is connected to the central piezoelectric elements. Phase FB is used for sensing the vibration state of an elastic body. The voltage is not applied to phase FB, and the voltage generated by the deformation of the piezoelectric elements is read when the elastic body vibrates. The vibration state of the elastic body can be seen according to this feedback (FB) voltage value.

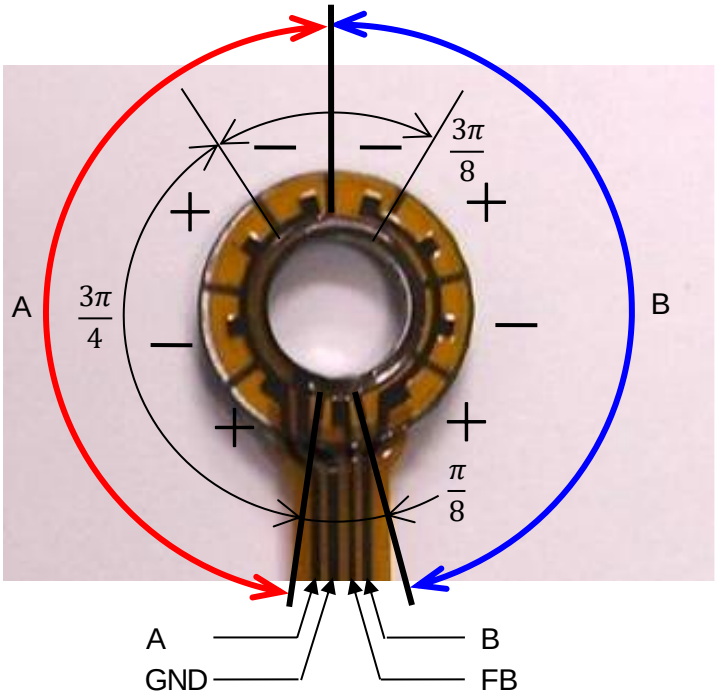


Fig. 2.5 Location of the piezoelectric elements.

The traveling wave is generated by the piezoelectric transverse effect of piezoelectric elements. As shown in Fig 2.6, the piezoelectric elements are polarized plus and minus. The plus polarized part expands in the circumferential direction and the minus polarized part contracts in the circumferential direction when the plus voltage is applied to the piezoelectric elements from the piezoelectric body to the elastic body. Conversely, the plus polarized part contracts in the circumferential direction and the minus polarized part expands in the circumferential direction when the minus voltage is applied. Therefore, the standing wave can be generated in the elastic body by applying AC voltage to the piezoelectric elements.

The phase A and phase B to which the voltage is applied are arranged by 1/4 wavelength shifted from each other. In this way, two standing waves with $\pi/2$ phase difference in the position are obtained. By applying the sine voltage whose phase difference is temporally shifted to the phase A and phase B, two standing waves with phase difference in the position and time are generated, and the traveling wave can be generated in the circumferential direction of the elastic body by the synthesis.

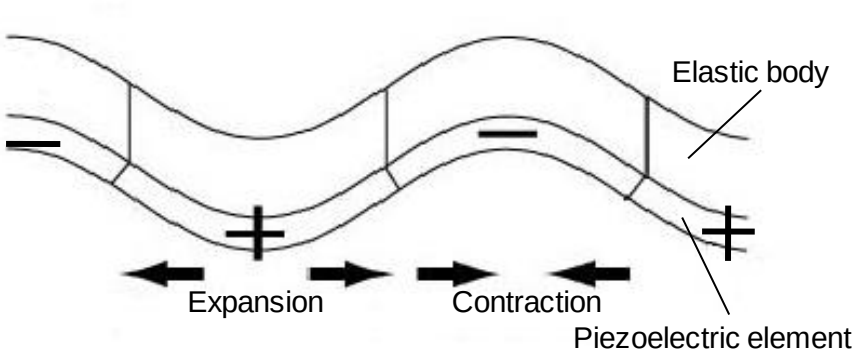


Fig. 2.6 Electrostriction behavior.

The spherical ultrasonic motor is composed of three annular vibrators and one spherical rotor, and the spherical rotor is held by three vibrators [22]. The schematic diagram is shown in Fig. 2.7. These three annular vibrators use the driving principle of the traveling wave type ultrasonic motor, and AC voltage is applied to the piezoelectric elements, and the traveling wave is generated on the surface of an elastic body by exciting ultrasonic vibration. The spherical rotor is in contact with the elastic body of the vibrator, so it receives the force around the axis of each circular ring by this traveling wave.

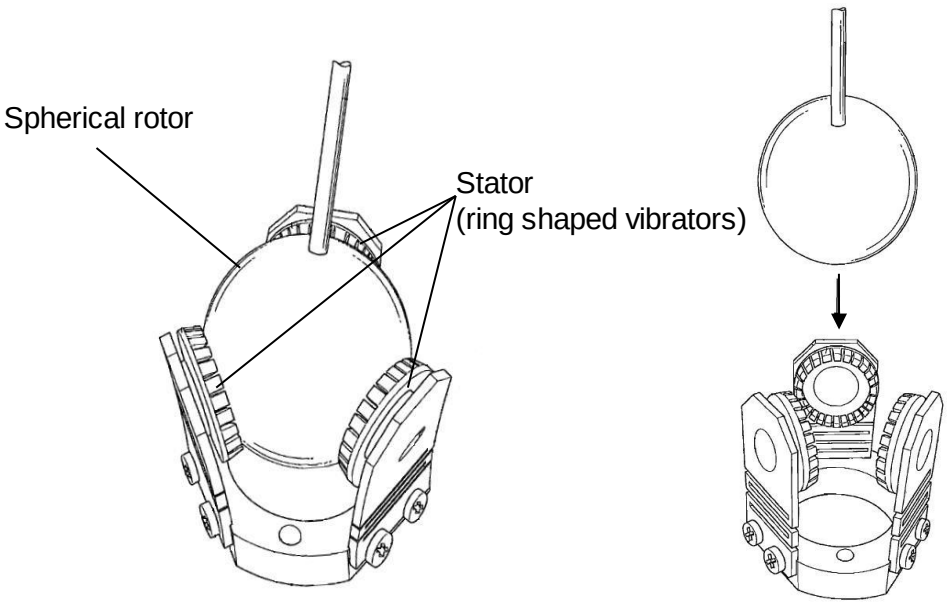


Fig. 2.7 Appearance of SUSM.

As shown in Fig. 2.8, the rotational vector of the spherical rotor is synthesized by the rotational vectors of each vibrator. The vibrators are arranged at an interval of 120° on the X-Y plane and are mounted on the Z axis direction on tilt of $\phi$. The torques $\mathbf{S}_1$, $\mathbf{S}_2$, and $\mathbf{S}_3$ applied by each vibrator to the sphere are geometrically expressed as follows from this arrangement:

$$\mathbf{S}_1 = T_1\left[\cos\frac{3}{2}\pi\cos\phi \quad \sin\frac{3}{2}\pi\cos\phi \quad \sin\phi\right]^T$$

$$\mathbf{S}_2 = T_2\left[\cos\frac{5}{6}\pi\cos\phi \quad \sin\frac{5}{6}\pi\cos\phi \quad \sin\phi\right]^T \tag{2.15}$$

$$\mathbf{S}_3 = T_3\left[\cos\frac{1}{6}\pi\cos\phi \quad \sin\frac{1}{6}\pi\cos\phi \quad \sin\phi\right]^T$$

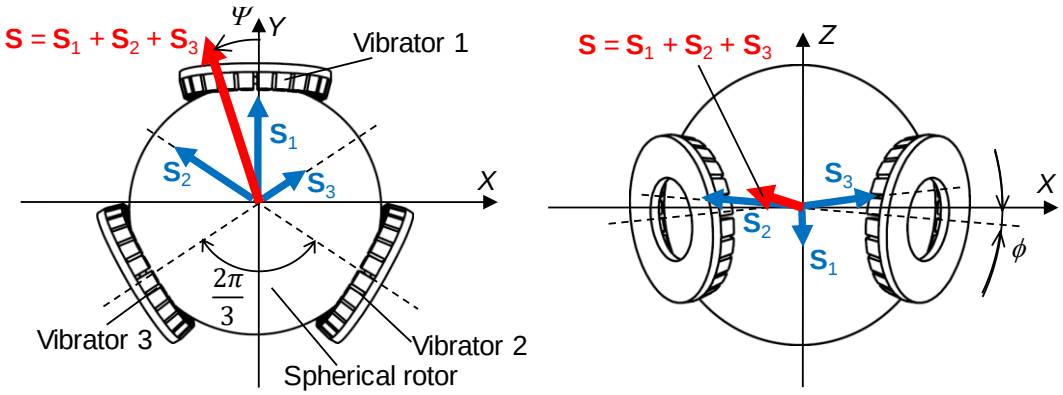


(a) X-Y plane (b) X-Z plane.

Fig. 2.8 Location of vibrators.

Where *T1*, *T2*, and *T3* are the torque magnitudes of each vibrator. The torque **S** of a spherical ultrasonic motor is expressed by the synthesis of the torques of each vibrator:

$$\mathbf{S} = \mathbf{S}_1 + \mathbf{S}_2 + \mathbf{S}_3 \tag{2.16}$$

$$\mathbf{S} = \begin{bmatrix} S_x \\ S_v \\ S_z \end{bmatrix} = \begin{bmatrix} \left( -\frac{\sqrt{3}}{2} T_2 + \frac{\sqrt{3}}{2} T_3 \right) \cos\phi \\ \left( -T_1 + \frac{1}{2} T_2 + \frac{1}{2} T_3 \right) \cos\phi \\ \left( T_1 + T_2 + T_3 \right) \sin\phi \end{bmatrix} \tag{2.17}$$

The torque of the sphere can be generated in any direction on the space by changing the torque magnitudes of each vibrator. That is, a spherical ultrasonic motor has three degree of freedom of rotation.

The holding torque exists and the posture is fixed as the spherical rotor is held by each vibrator at no power supply. At this time, it is also possible to create a state in which the sphere can hardly rotate in either direction and no holding torque exists by generating a standing wave in each vibrator.

In addition to the above characteristics, a spherical ultrasonic motor takes over the characteristics of an ultrasonic motor [35], so it has some advantages compared with an electromagnetic motor. The characteristics of a spherical ultrasonic motor are described below.

1) It has three degree of freedom of rotation.

2) The mechanism is simple, and the reducer is unnecessary, so it is excellent in space saving.

3) It is direct drive by friction, and it is low speed and high torque, and it has very high responsiveness.

4) There is a holding torque at no power supply, so the brakes are not necessary.

5) It is not driven by electromagnetic force, so it can hardly receive the actions of electric fields and magnetic fields.

Due to the characteristic of 5), it is possible to correspond to the MRI (Magnetic Resonance Imaging) environment by using nonmagnetic material in the constituent material of spherical ultrasonic motor.

### 2.1.3. Ultrasonic motor with coil stator

A basic configuration of an ultrasonic motor with coil stator is shown in Fig 2.9. This ultrasonic motor with coil stator is composed of three parts: cylindrical rotor, wire with one end of coil shape, and vibration source [36]. The wire is a waveguide for transmitting ultrasonic vibration, and the coil part plays the role of the stator.

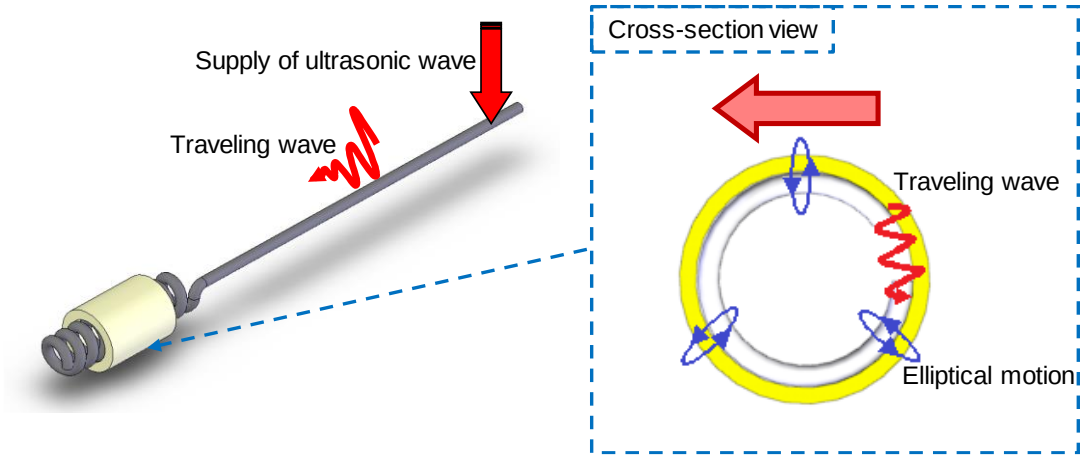


Fig. 2.9 Principle of ultrasonic motor with coil stator.

The ultrasonic vibration becomes a traveling wave and propagates to the coil stator through the waveguide when ultrasonic vibration is applied to the waveguide from the vibration source. At this time, the traveling wave propagated to the coil stator as described in the previous section, elliptical motion is generated at the mass point on the coil stator surface. Friction force is generated by this elliptical motion between the coil stator and rotor, and the rotor performs rotational motion.

However, the direction in which the elliptical motion generates is opposite to the traveling direction of the traveling wave, so the rotor rotates in the direction opposite to the winding direction of the coil stator. In addition, when the pitch angle of the coil stator is $\phi$, this elliptical motion causes a force to deviate the rotational direction of rotor by that angle. The image is shown in Fig. 2.10. The friction force due to this elliptical motion can be divided into the radial force of rotating the rotor and the axial force of the rotor. Therefore, the rotor also performs rotation simultaneously with axial translation.

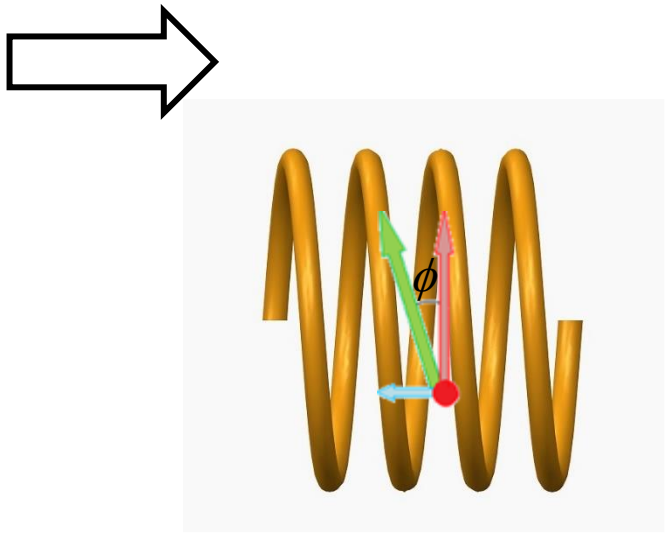


Fig. 2.10 The power of translation direction of coil motor.

As a feature of this ultrasonic motor with coil stator, ultrasonic vibration is transmitted to the driving part through the waveguide, so the driving part and the vibration source can be separated by changing the length of the waveguide, and the remote operation is possible. In addition, in the support of the rotor, it is supported by the fitting of the rotor and the coil stator, so the preload spring is unnecessary, and it can be said that it is a motor suitable for the miniaturization as the number of parts is small.

Many parameters are involved in the generation of driving force of the ultrasonic motor with coil stator. Regarding these parameters, the amplitude and frequency of the ultrasonic vibration, the preload acting between the stator and the rotor, the friction coefficient, the wear, the rigidity ratio, and the acoustic impedance of the coil stator and waveguide can be clarified. The state of contact between the traveling wave and the rotor is shown in Fig. 2.11. Here, it can be assumed that the deformation of the wave due to the contact with the rotor can hardly occur, and $P$ is the preload, and $\mu$ is the coefficient of friction, and $\Delta y$ is the displacement given by the traveling wave, and $k_y$ is the longitudinal rigidity ratio. Details of each parameter are shown below.

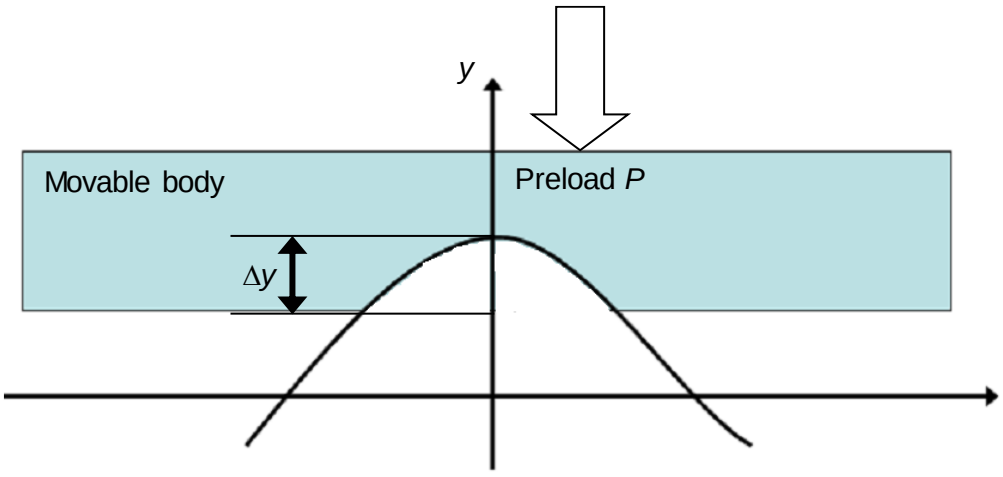


Fig. 2.11 Contact with movable body and traveling wave.

(a) Amplitude and frequency of ultrasonic vibration

The amplitude of the ultrasonic vibration determines the contact area of the traveling wave and the rotor. This contact area is optimized by the appropriate value of the amplitude, and stable driving force can be obtained.

It can be considered that the frequency of the ultrasonic vibration determines the wave number in contact with the rotor, so it is closely related to the driving force. In addition, this frequency is closely related to the intrinsic frequency of the stator. The phenomenon in which the frequency of the input ultrasonic vibration coincides with the intrinsic frequency is generally called a resonance, and the frequency at that time is called a resonance frequency. It can be clarified that the vibration is amplified in the resonance and it can be said that it is an important parameter in not only the ultrasonic motor with coil stator but also the ultrasonic motor, and the resonance frequency depends on the shape, and it can be considered useful to perform analysis using the finite element method in order to avoid the phenomenon such as surging [37].

(b) Preload acting between stator and rotor

In the ultrasonic motor, it is necessary to increase the friction force by pressing the rotor against the generated wave and to obtain the driving force efficiently. This pressing force is called preload. The preload is related to the sinking amount into the rotor, that is, the contact area between the rotor and the stator. The force transmitted from the stator increases by increasing preload and increasing the sinking amount. However, the elliptical motion of the mass point on the surface of the elastic body which becomes a driving force is in opposite direction at the part of the wave crest and wave trough. Therefore, the friction in that part acts as a resistance force against the driving direction when the rotor is in contact with the trough part. Therefore, it can be reported that the driving force improves by setting the preload to an appropriate value.

Here, the elliptical motion of the mass point on the surface of the elastic body is focused on. The $x$ direction velocity of the mass point performing the elliptical motion which can be calculated by differentiating the equation (2.6) is shown in the equation (2.18). However, $V_x$ is the $x$ direction velocity of the mass point which performs the elliptical motion:

$$V_x = H \cdot A \cdot \omega \cdot \frac{2\pi}{\lambda} \cdot \sin\left( \frac{2\pi}{\lambda} x_m + \omega t \right) \tag{2.18}$$

From the equation (2.18), $V_x$ in the range of $+y$ is maximum at the vertex of the wave, and it decreases with decreasing $y$, and it becomes $V_x = 0$ in $y = 0$. Here, it can be considered that the preload is large and the sinking amount is large as shown in Fig. 2.12. However, the traveling direction of the traveling wave is the $+x$ direction and the moving speed of the rotor is $V$. At this time, the driving force is exerted by friction from the entire contacting area by the sinking at the time of rising of the rotor ($V = 0$). However, when the rotor is accelerated and reaches a certain velocity $V'$, if the position $V_x = V'$ is $y_{V'}$, the movement speed of the mass point relative to the moving speed of the rotor becomes relatively slow in the range of $y < y_{V'}$, and the driving resistance acts from the contact surface. From the above, it is important to make the preload with an appropriate value when transmitting the force efficiently from the traveling wave.

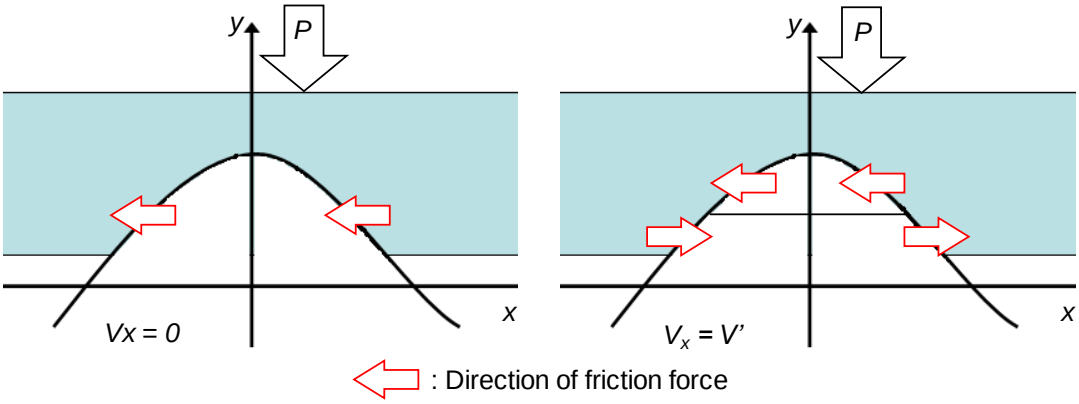


Fig. 2.12 Distinction of friction force.

(c) Friction coefficient, wear, and rigidity ratio

The friction coefficient and the rigidity ratio of the rotor are determined by the respective materials of the rotor and the stator. The ultrasonic motor is a motor to obtain driving force from friction, and it can be considered that stabilization of driving force can be achieved by optimization of the friction coefficient. However, the friction coefficient shown here does not refer only to a combination of materials, but it is determined by a plurality of factors such as the surface roughness, the contact state, the contact area of each stator and rotor, so individual tests are required to calculate as a concrete numerical value. In this way, it is necessary to consider the wear as it is driven mainly by the friction force. When the wear progresses, the contact state between the stator and the rotor and the surface roughness change, which leads to a decrease of the driving force and a decrease of the life.

As described above, in order to improve the driving force of an ultrasonic motor, it is necessary to determine the materials of the stator and the rotor in consideration of friction coefficient and the wear.

(d) Intrinsic acoustic impedance of the coil stator and waveguide

The ultrasonic motor with coil stator adopts the method to propagate ultrasonic vibration to the driving part through the waveguide. Therefore, it can be considered that the propagation efficiency of the ultrasonic vibration affects the driving. Among them, it is necessary to consider the intrinsic acoustic impedance which is the acoustic resistance generated in the medium when ultrasonic vibrations are propagated.

The propagation speed of ultrasonic vibration is faster in solid than in liquid, and faster in liquid than in gas. This is because the intrinsic acoustic impedance of solid is larger than that of liquid, and that of liquid is larger than that of gas. The value of the intrinsic acoustic impedance $Z_0$ is expressed by the following equation (2.19). However, $\rho$ is the density of the propagation medium and $C$ is the acoustic velocity.

$$Z_0 = \rho C \tag{2.19}$$

In addition, the intrinsic acoustic impedance is shown in Table 2.1. However, the density is $\rho$ [$\times 10^3$ kg/m$^3$], and the acoustic velocity is $C$ [m/s], and the intrinsic acoustic impedance is $Z_0$ [$\times 10^6$ N・s/m$^3$].

It is necessary to determine the blocking layer in consideration of this intrinsic acoustic impedance when driving the ultrasonic motor with coil stator. The propagation efficiency can be enhanced by setting the difference between the values of the intrinsic acoustic impedance of the blocking layer and the waveguide when propagating the ultrasonic vibration through the waveguide.

Table 2.1 Acoustic impedance by material.

| Material | Density $\rho$ | Acoustic velocity $C$ | Acoustic impedance $Z_0$ |
|---|---|---|---|
| Air | 1.2 | 340 | 408 |
| Water | 1000 | 1440 | $1.44\times10^6$ |
| Flexible rubber | 950 | 70 | $0.067\times10^6$ |
| Quartz | 2700 | 4400 | $12\times10^6$ |
| Aluminum | 2700 | 5200 | $14\times10^6$ |
| Steel | 7700 | 5000 | $39\times10^6$ |
| SUS | 7910 | 5790 | $45.7\times10^6$ |
| Tungsten | 19200 | 5410 | $103\times10^6$ |

## 2.2. Spherical ultrasonic motor using wire stators

The spherical ultrasonic motor using wire stators is being developed in this study is a kind of the multi degree of freedom motors. A multi degree of freedom motor refers to a motor capable of movement of two or more degree of freedom. There are six degree of freedom in total, translational three degree of freedom and rotational three degree of freedom, in the motion of a rigid body in the three dimensional space. Using one degree of freedom motor and attaining these motions require at least one motor for one degree of freedom. On the other hand, it is possible to reduce the number of motors by using a multi degree of freedom motor. This not only has the effect of simplifying the design and structure but also the reduction of the self-weight of the equipment, and the energy consumption decreases and energy saving effect is generated. Among them, the spherical motor has three degree of freedom of rotation of each one, so the effect of them can be considered to be large. The advantages of the spherical motor are shown below [38].

(1) The number of motors required to realize the same degree of freedom is reduced, and the miniaturization and lightening of the motor can be realized.
(2) Energy saving effect is great as the number of motors used in the system can be reduced.
(3) The equation of motion is simplified and the control can be performed simply and at high speed as the rotational center is coincident.
(4) The robot eye drive unit and the active joint part of the truss structure can be configured without adding extra mechanism.

### 2.2.1. Structure of spherical ultrasonic motor using wire stators

In this study, the stator shape of the ultrasonic motor with coil stator mentioned above is changed and the application to the spherical ultrasonic motor can be considered. This stator is called a spherical ultrasonic motor using wire stators.

The basic structure is shown in Fig. 2.13. This motor is composed of one spherical rotor and four traveling wave ultrasonic motor stators. The four stators have two pairs and each pair is arranged to face to each other on the diagonal line. Supposing that these two diagonal lines can be assumed to be $x$ axis and $y$ axis, two rotational degree of freedom is performed by the synthesis of the rotational vectors when a force is generated to rotate the rotor around each axis in two pairs of stators [39].

The degree of freedom required for driving the camera of the coronary angioscopy with spherical ultrasonic motor using wire stators is two degree of freedom and simple driving control of two axes, so the structure using four stators is adopted in this study.

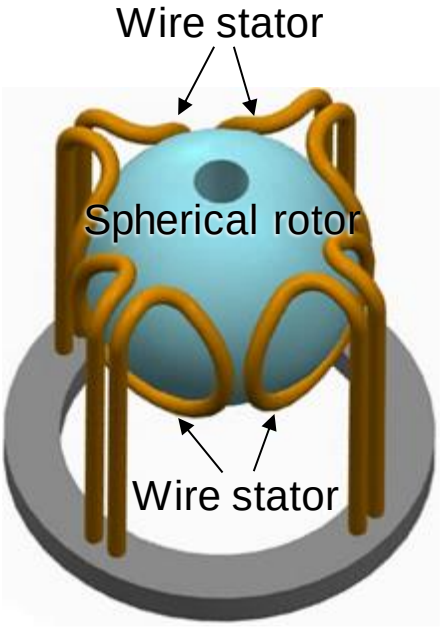


Fig. 2.13 Spherical ultrasonic motor using wire stators.

### 2.2.2. Driving principle of spherical ultrasonic motor using wire stators

This spherical ultrasonic motor using wire stators can rotate the disk and the spherical rotor by making the stator shape into a ring shape or a spiral shape. A structure of a spherical ultrasonic motor using a wire stator is shown in Fig. 2.14. The driving principle is similar to that of the ultrasonic motor with coil stator, and the traveling wave is generated by applying ultrasonic vibration to the waveguide part extended from the stator part, and the rotor rotates by the elliptical motion on the stator surface.

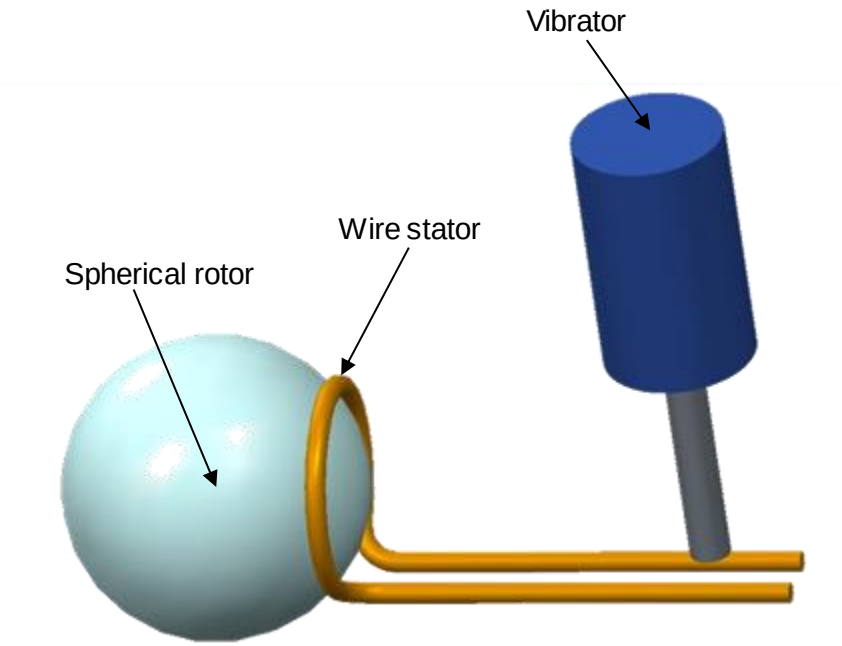


Fig. 2.14 Spherical ultrasonic motor using a wire stator.

The stator used in the conventional spherical ultrasonic motor has a structure in which the piezoelectric elements as vibration sources are pressed against the elastic body, so problems such as the manufacturing limit of the piezoelectric elements occur in miniaturization. On the other hand, the spherical ultrasonic motor using wire stators has the structure to transmit ultrasonic vibration to the stator part through the waveguide of the wire, so it is possible to pursue the miniaturization without being influenced by the size of the vibration source. In addition, when considering the use as a coronary angioscopy, it is necessary to apply the voltage to the piezoelectric elements when driving the conventional ultrasonic motor which can be considered to be dangerous when used in the body. On the other hand, spherical ultrasonic motor using wire stators can be driven by applying vibration from the outside of the body which can be said to be superior from the aspect of safety.

### 2.2.3. Shape of wire stator

In the previous study [40-41], two types of ring and spiral types have been proposed as stator shapes of spherical ultrasonic motor using wire stators as shown in Fig. 2.15. The ring type stator shown in Fig. 2.15 (a) has a structure in which the waveguide is extended from a ring type wire. As the advantage of ring type, it can be miniaturized for its simple structure. In addition, it is also advantageous that the non-uniformity of the contact surface can hardly occur as the spherical rotor is supported by one loop. On the other hand, as the disadvantage of ring shape, the driving force is declined by the decrease of the contact surface.

The spiral type stator shown in Fig. 2.15 (b) has a structure in which the waveguide is extended from the spiral wire. As the advantage of spiral type, the loop supporting the spherical rotor increases, so the contact surface increases and the driving force is improved. In addition, one end of the waveguide is located at the center of the stator, so it is also advantageous that the pressing force can be applied. On the other hand, the spiral is not suitable for miniaturization due to the large numbers of loops.

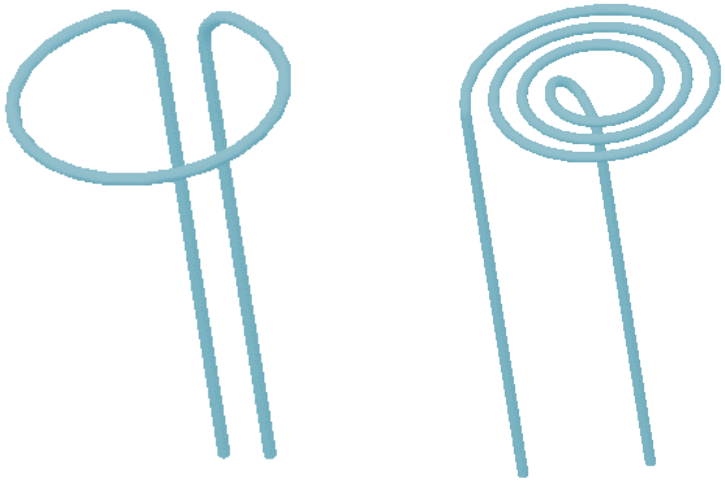

(a) Ring type stator (b) Spiral type stator

Fig. 2.15 Shape of wire stator.

In consideration of the above, the spiral type stator of approximately one spiral is used in this study as shown in Fig. 2.16. The wire stator used in the experiment is shown in Fig. 2.16 (a). The wire stator is stainless steel (SUS304), and the maximum diameter is 10 mm. About the wire diameter, the experiment and examination on 0.3 mm and 0.5 mm have been carried out in Toyama laboratory at the Tokyo University of Agriculture and Technology. The wire diameter of this experiment is 0.5 mm since it can be known that the influence due to the difference in the wire diameter is small. The length of the waveguide is 30 mm. Asymmetry of shape can be considered, and two types of left spiral and right spiral are designed. In addition, there are two waveguides in the outside and inside wire stators. By changing the waveguide connected with the vibration source, the direction of traveling wave changes, and the rotational direction of the spherical rotor can be reversed. In this study, the case where the vibration source is connected to the outside waveguide is forward rotation as shown in Fig. 2.16 (b), and the case where the vibration source is connected to the inside waveguide is reverse rotation as shown in Fig. 2.16 (c).

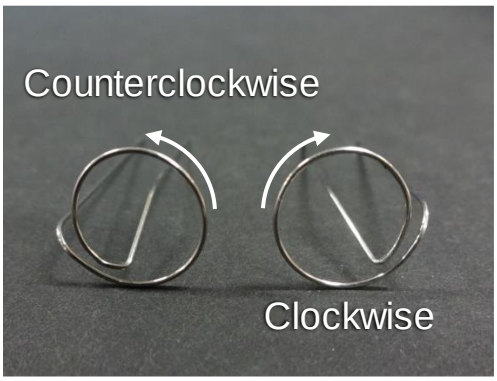


(a) Winding pattern

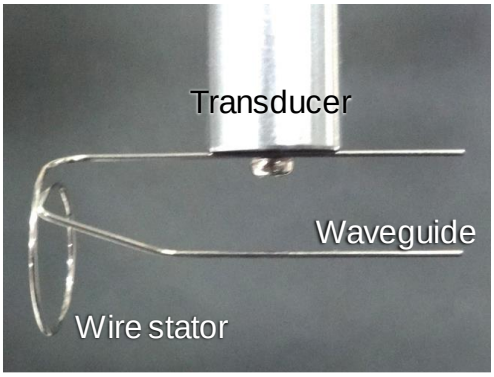


(b) Connection of forward rotation

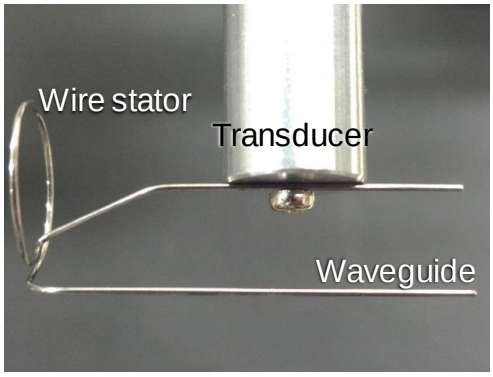


(c) Connection of reverse rotation

Fig. 2.16 Wire stator of single spiral.

# Chapter 3. Fundamental characteristics of spherical ultrasonic motor

In this chapter, the pressing force and the starting torque between a stator and a spherical rotor which are important when developing a miniature spherical ultrasonic motor are discussed.

## 3.1. Pressing force of spherical ultrasonic motor using wire stators

### 3.1.1. Relationship between pressing force and pressing distance

The experimental equipment shown in Fig. 3.1 is prepared to investigate the relationship between the pressing force and the pressing distance. The experimental equipment is composed of an X stage and a spherical ultrasonic motor. A load cell is mounted to the X stage. The spherical ultrasonic motor is composed of one spherical rotor, one wire stator, and one vibration source. The waveguide of the wire stator is screwed to the tip of the Langevin transducer which is the vibration source, and the vibration applied from the vibrator to the waveguide is transverse vibration.

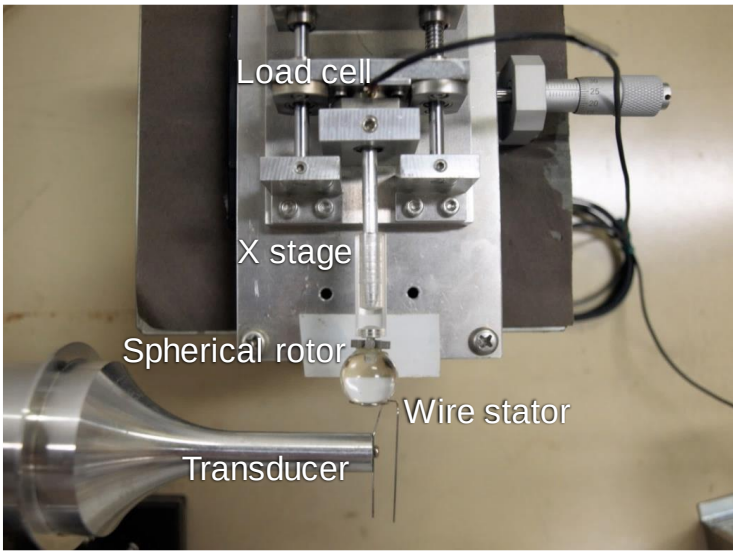


Fig. 3.1 Experimental equipment of pressing force measurement.

One part of the spherical rotor is in contact with the wire stator, and the other part is in contact with the X stage. The X stage is pressed against the spherical rotor while measuring the distance using a micrometer, and the output voltage of the load cell for the pressing distance is recorded. The relationship between the pressing force and the pressing distance in the case where the wire stator of forward rotation connection and reverse rotation connection is used as shown in Fig. 3.2. Large difference due to the connection state cannot be seen, so the pressing distance is converted to the pressing force using the following approximate straight line:

$$F_P = 0.26 \times D_P \tag{3.1}$$

Where $F_p$ is the pressing force, and $D_p$ is the pressing distance.

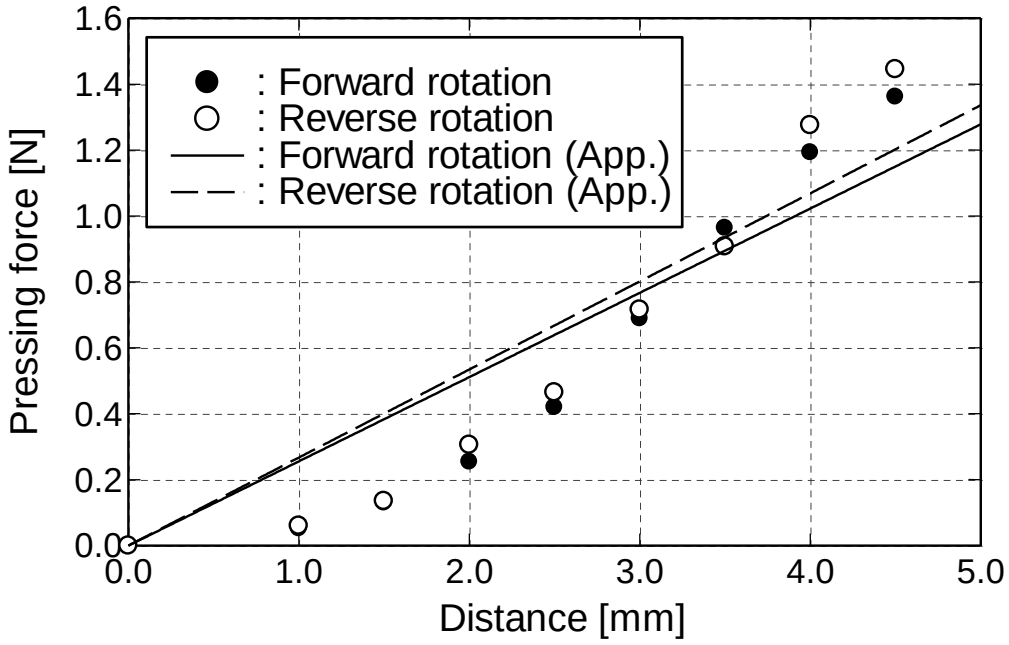


Fig. 3.2 Relationship between pressing distance and pressing force.

### 3.1.2. Experimental method on pressing force and rotational speed

The experimental equipment shown in Fig. 3.3 is used to investigate the optimum pressing force. The experimental equipment is composed of a spherical ultrasonic motor, an XYZ stage, a waveform generator (WF1974, NF Corporation), and an amplifier (BA4825, NF Corporation). The spherical ultrasonic motor is one axis, which is composed of one spherical rotor, two wire stators, and two Langevin transducers of vibration source. The material of the spherical rotor is polycarbonate and the diameter is 15 mm. The waveguide of wire stator is located at the tip of the Langevin transducer. One part of the Langevin transducer is fixed, and the other part is located on the XYZ stage so that the position can be changed.

The AC voltage with amplitude and frequency control is sent from the waveform generator to the amplifier, and the voltage is applied to the Langevin transducer vibrating the wire stator. The vibration frequency is 24.6 kHz equal to the resonance frequency of the Langevin transducer. In addition, the position where the spherical rotor contacts the wire stator (pressing force = 0 N) can be assumed to be 0 mm as the reference point of the pressing position. The micrometer of the XYZ stage is applied to move one wire stator in parallel at 0.1 mm intervals, and the rotational speed is measured with increasing pressing force. The measuring range of the rotational speed of the spherical rotor which can be held properly by the wire stator is from 2.0 mm to 4.0 mm. Through the above operation, the amplitude of the AC voltage is changed from 10 $V_{p\text{-}p}$ to 70 $V_{p\text{-}p}$ at 10 $V_{p\text{-}p}$ intervals, and forward rotation and reverse rotation are respectively carried out. The pressing distance is converted to the pressing force by the approximate straight line from Equation (1). The rotational speed is obtained from the experimental video taken by the video camera. The rotational speed of the rotor is obtained from the video taken by a video camera. The frame rate of the video camera is 30 fps.

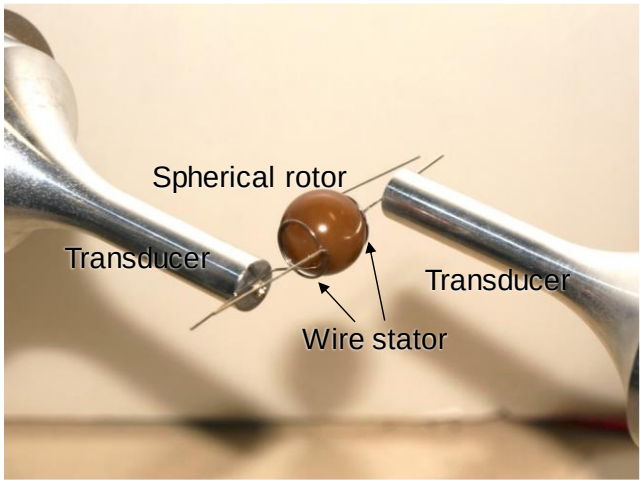


Fig. 3.3 Experimental equipment of rotational speed measurement.

### 3.1.3. Experimental result on pressing force and rotational speed

The measuring results of the rotational speed with respect to the pressing force in the case where the method of mounting the wire stator is forward rotation are shown in Fig. 3.4. The number of measuring points is small in the case where the amplitude of AC voltage is 10 $V_{p\text{-}p}$, as the rotation stops before pressing to the specified position. As shown in Fig. 3.4(a), the rotational speed increases uniformly when the amplitude of AC voltage is increased from 10 $V_{p\text{-}p}$ to 40 $V_{p\text{-}p}$. In addition, the rotational speed decreases with increasing the pressing force. As shown in Fig. 3.4(b), the rotational speed decreases slightly with the pressing force in the range of 0.7 N or less when the amplitude of AC voltage is increased from 50 $V_{p\text{-}p}$ to 70 $V_{p\text{-}p}$. However, the rotational speed increases with the pressing force in the range of 0.7 N or more. In addition, the rotational speed decreases with increasing pressing force.

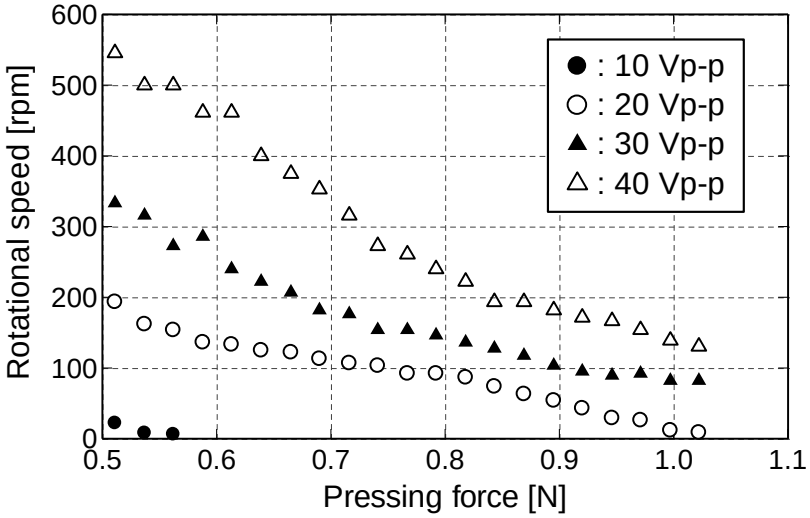


(a) 10 $V_{p\text{-}p}$ ~ 40 $V_{p\text{-}p}$

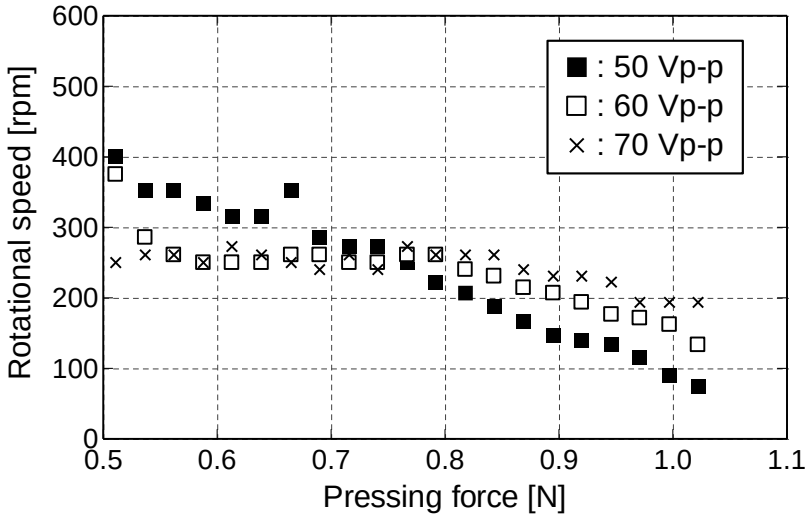


(b) 50 $V_{p\text{-}p}$ ~ 70 $V_{p\text{-}p}$

Fig. 3.4 Relationship between pressing force and rotational speed (forward rotation).

On the other hand, the measuring results of the rotational speed with respect to the pressing force in the case where the method of mounting the wire stator is reverse rotation are shown in Fig. 3.5. The number of measuring points is small in the case where the amplitude of AC voltage is 10 $V_{p\text{-}p}$, as the rotation stops before pressing to the specified position. As shown in Fig. 3.5(a), the rotational speed increases uniformly when the amplitude of AC voltage is increased from 10 $V_{p\text{-}p}$ to 40 $V_{p\text{-}p}$. In addition, the rotational speed tends to decrease, but it tends to increase in the middle when the pressing force is increased. As shown in Fig. 3.5(b), the rotational speed decreases slightly with the pressing force in the range of 0.7 N or less when the amplitude of AC voltage is increased from 50 $V_{p\text{-}p}$ to 70 $V_{p\text{-}p}$. However, the change of the rotational speed is small with the pressing force in the range of 0.7 N or more. In addition, the rotational speed tends to decrease first and then increase when the pressing force is increased in the range of 0.7 N or less. However, the fluctuating of the rotational speed decreases when the pressing force is increased in the range of 0.7 N or more.

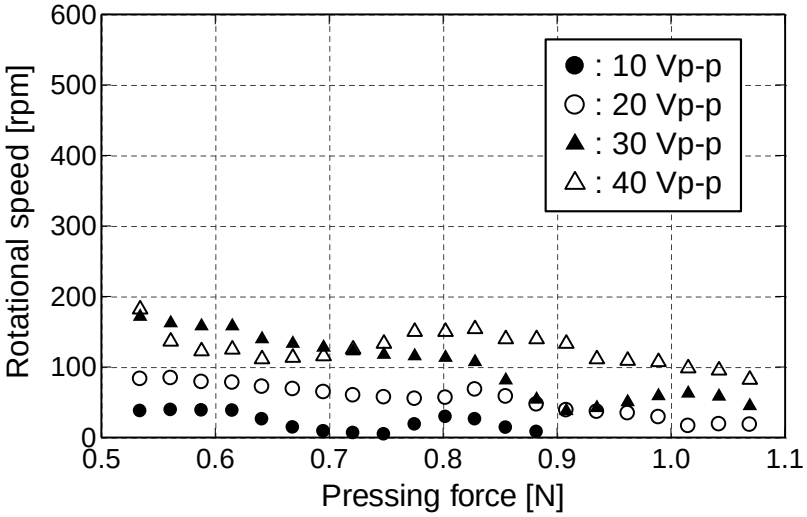


(a) 10 Vp-p ~ 40 Vp-p

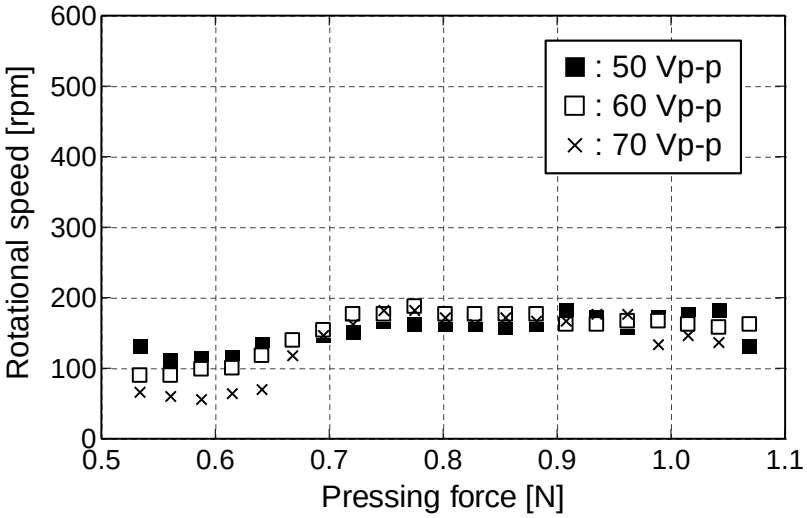


(b) 50 $V_{p\text{-}p}$ ~ 70 $V_{p\text{-}p}$

Fig. 3.5 Relationship between pressing force and rotational speed (reverse rotation).

Comparing with Fig. 3.4 and Fig. 3.5, it can be seen that the rotational number and tendency are different between forward rotation and reverse rotation. The difference in the characteristics of forward rotation and reverse rotation of the rotor is due to the asymmetric shape of the wire stator. In the experiment of this chapter, it can be considered that the characteristics are greatly different since the mounting method with the Langevin transducer is also carried out side by side. The first contact is inside of the spiral when the wire stator is made to approach the spherical rotor. In the case of forward rotation in which the outside waveguide is connected, the pressing force is transmitted uniformly to the inside in order to press the spherical rotor from the outside of the stator. On the other hand, in the case of reverse rotation in which the inside waveguide is connected, the pressing force is transmitted non-uniformly to the outside in order to press the spherical rotor from the inside of the stator. Therefore, it can be considered that the distribution of the friction force transmitted from the wire stator to the spherical rotor is different between forward rotation and revere rotation. Then, both waveguides are used when the wire stator is pressed against the spherical rotor.

In this study, it can be assumed that a miniature spherical ultrasonic motor is used for the coronary angioscopy. The actual waveguide is longer than the experimental equipment and the damping of the traveling wave is expected, so the output can be as large as possible. Therefore, the amplitude of the voltage is approximately 40 $V_{p\text{-}p}$ in forward rotation, and it is suitable when the pressing force is approximately 0.5 N. The amplitude of the voltage is approximately 60 $V_{p\text{-}p}$ in the case of reverse rotation, and it is suitable when the pressing force is approximately from 0.7 N to 0.8 N.

## 3.2. Starting torque of spherical ultrasonic motor

### 3.2.1. Measuring method of starting torque

In order to measure the starting torque, the weights are attached to the spherical rotor of the experimental equipment through a string as shown in Fig. 3.3. The Langevin transducer with resonance frequency of 24.6 kHz is used as the ultrasonic vibration source.

In this experiment, the starting torque of the spherical rotor is respectively measured for both forward rotation and reverse rotation by changing the frequency and amplitude of the applied AC voltage. The load of the weights is mounted to the motor without driving from 1000 mg, the load is reduced by 10 mg, and the starting torque is calculated from the load when the spherical rotor begins to rotate. First, the applied voltage of the Langevin transducer is fixed to 40 $V_{p\text{-}p}$, and the starting torque is measured by changing the applied frequency from the resonance frequency by 0.005 kHz. Next, the applied frequency of the Langevin transducer is fixed to 24.6 kHz which is the same as the resonance frequency, and the starting torque is measured by changing the applied voltage from 10 $V_{p\text{-}p}$ to 70 $V_{p\text{-}p}$ by 10 $V_{p\text{-}p}$.

### 3.2.2. Experimental result on starting torque

The starting torque is shown in Fig. 3.6 when the frequency is changed. The starting torque is maximum regardless of the rotational direction when the applied frequency is the resonance frequency of the Langevin transducer. In addition, the starting torque decreases when the applied frequency leaves the resonance frequency. The starting torque is shown in Fig. 3.7 when the amplitude of the voltage is varied. The starting torque is high when the amplitude of the voltage is small, and the starting torque decreases from 20 $V_{p\text{-}p}$ in forward rotation and from 30 $V_{p\text{-}p}$ in reverse rotation. However, after the starting torque decreases, the starting torque increases again as the amplitude of the voltage increases.

The influence of the friction force can be considered as the cause of the tendency as shown in Fig. 3.7. The vibration at the surface of the wire stator decreases when the amplitude of the voltage is small. It can be considered that the static friction force between the wire stator and the spherical rotor acts and the starting torque increases. On the other hand, the vibration at the surface of the wire stator becomes large when the amplitude of the voltage is large. It can be considered that the dynamic friction force between the wire stator and the spherical rotor acts and the starting torque decreases. However, the reason for the starting torque increasing again after decreasing is that the vibration at the surface of the wire stator becomes large when the amplitude of the voltage increases in the range of the dynamic friction force and the cause of the increase of the friction force can be considered to be the increase of the contact part with the spherical rotor.

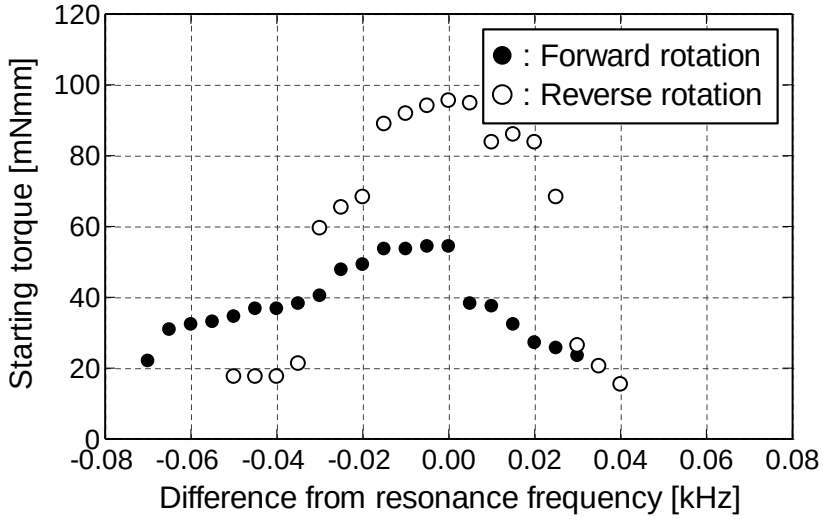


Fig. 3.6 Relationship between frequency of AC voltage and starting torque.

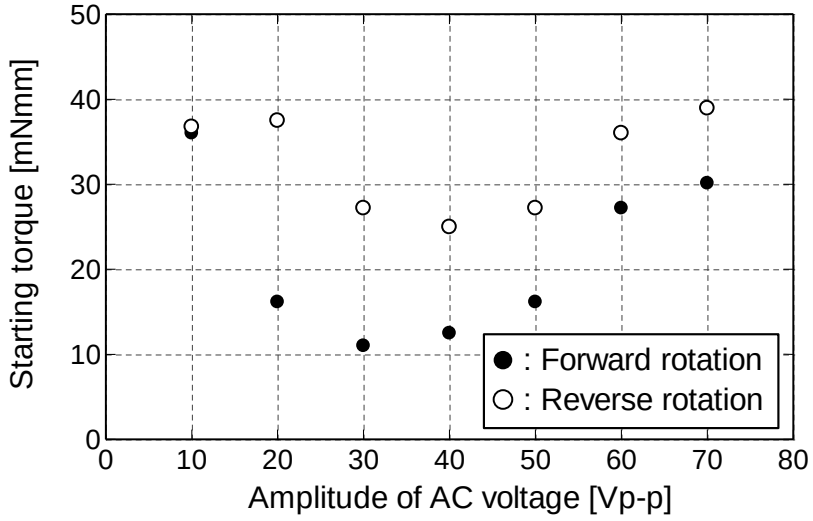


Fig. 3.7 Relationship between amplitude of AC voltage and starting torque.

## 3.3. Summary of chapter 3

First, the pressing force which is an important factor in developing an ultrasonic motor is investigated. The relationship between the pressing force and the rotational number is investigated, and it can be clarified that there is an optimum value for the pressing force, and there is a difference between forward rotation and reverse rotation. Next, the starting torque which is one characteristic of the motor is investigated. The relationship between the frequency and amplitude of the AC voltage applied and the starting torque is investigated, and it can be clarified that there is a difference between forward rotation and reverse rotation.

The ultimate goal of this study is to develop a new coronary angioscopy. The added value of the new coronary angioscopy is that the lesion can be photographed in the center of the image at the observation of the blood vessel lumen. For this purpose, it is necessary to drive the camera of the coronary angioscopy by a motor. The miniature spherical ultrasonic motor using wire stators is used as the motor. The fundamental study on the coronary angioscopy conducted in this study aims to investigate the items related to the miniature motor in the development items of the coronary angioscopy. The results in this chapter can be applied to the mounting position where optimum pressing force is obtained for the spherical rotor and wire stator and the optimum voltage value required while driving the miniature motor. In addition, a high rotational speed can be expected and the voltage of 40 $V_{p\text{-}p}$ with small starting torque is used in actual design.

# Chapter 4. Control of spherical ultrasonic motor

In this chapter, the control method of the rotational direction of a spherical ultrasonic motor using wire stators is discussed. A PWM control method is proposed to control the rotational direction of an ultrasonic motor.

## 4.1. Application of PWM control on spherical ultrasonic motor

Two degree of freedom drive of spherical ultrasonic motor using wire stators is made by synthesizing the driving forces of two sets of axes when the waveguide is connected vertically to the vibration source. In the previous study [41], the rotational direction is controlled in eight directions by synthesizing the driving forces of forward rotation and reverse rotation with the same size. The rotational direction of the eight directions by synthesizing the driving forces is shown in Fig. 4.1 and Table 4.1. In this study, a control method to obtain the rotational direction in all directions is proposed. With synthesizing the driving forces of two sets of axes, the rotational direction changes according to the difference of the driving forces when the difference is given to the driving forces. A method to increase or decrease the amplitude of the traveling wave generated on the one axis can be considered as a method of giving the difference to the driving forces. However, the friction force between the wire stator and the spherical rotor increases with the smaller amplitude and prevents driving, so it is not suitable for the control of the rotational direction. In this study, the PWM control method used in the control of an electromagnetic motor is applied to an ultrasonic motor. Using this method, it is possible to change the driving force transmitted to the spherical rotor without changing the friction force between the wire stator and the spherical rotor.

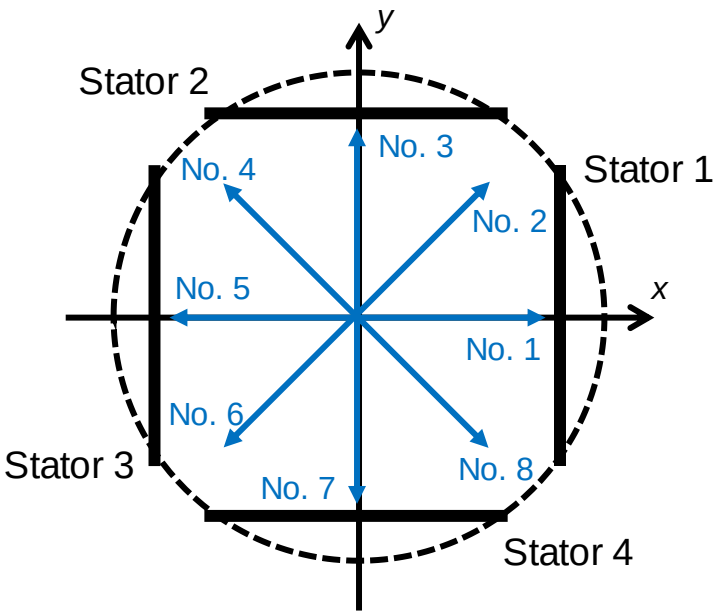


Fig. 4.1 Schematic diagram of rotational direction.

Table 4.1 Driving direction and rotational direction.

| No. | Driving direction | | Rotational direction |
|---|---|---|---|
| | Stator 1 & 3 | Stator 2 & 4 | |
| 1 | without driving force | Forward | Right |
| 2 | Forward | Forward | Upper right |
| 3 | Forward | without driving force | Upper |
| 4 | Forward | Reverse | Upper left |
| 5 | without driving force | Reverse | Left |
| 6 | Reverse | Reverse | Lower left |
| 7 | Reverse | without driving force | Lower |
| 8 | Reverse | Forward | Lower right |

PWM control used in an electromagnetic motor is a method of controlling the output of an electromagnetic motor by switching the constant voltage on and off. A constant period of on and off of a pulse sequence is made from the input of a constant voltage, and an arbitrary voltage proportional to the pulse width of on is obtained by rapid periodic switch. The driving principle is different between an ultrasonic motor and an electromagnetic motor, so it is difficult to use the same principle. Therefore, two application methods can be considered. The first method is to control the voltage of the wire stator by switching the AC voltage on and off applied to the ultrasonic vibration source like the electromagnetic motor. The second method is to switch the standing wave without driving force to the traveling wave and the spherical rotor on the wire stator. In the former, it can be concerned that the friction force between the wire stator and the spherical rotor increases at the timing when the voltage turns off. In this study, the latter method is focused on.

How to switch the traveling wave and the standing wave on the wire stator is explained. One wire stator has two waveguides, so vibration sources are connected to respective waveguide. The connection between the vibration source and the waveguide is shown in Fig. 4.2. The traveling wave is generated on the wire stator in forward rotation when the vibration source connected to the outside waveguide is operated. The traveling wave is generated on the wire stator in reverse rotation when the vibration source connected to the inside waveguide is operated. Traveling waves are synthesized on the wire stators to generate the standing wave when two vibration sources are operated simultaneously. Therefore, the traveling wave and the standing wave can be switched by the operation state of the vibration source.

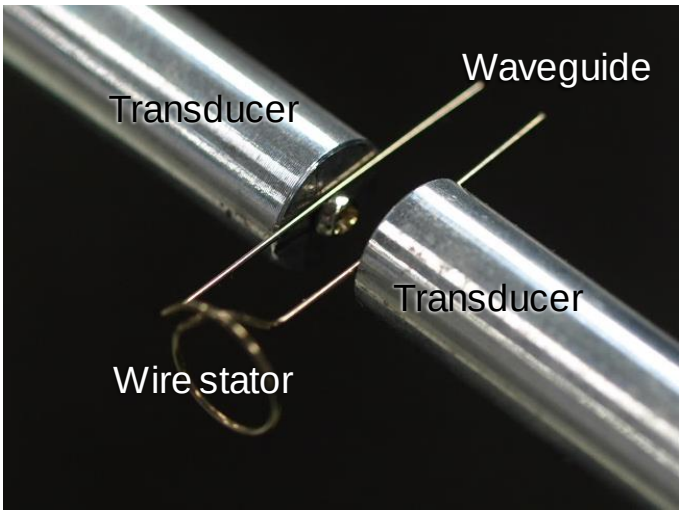


Fig. 4.2 Connection between transducer and waveguide.

The driving force is obtained by the duty ratio proportional to the time in which the traveling wave occurs in the period of generating the traveling wave and the standing wave when the input on state of PWM control is the traveling wave and the off state is the standing wave. One vibration source connected to the wire stator constantly generates traveling waves, while the other vibration source vibrates by the duty ratio. In addition, the standing wave can hardly generate a friction force against the spherical rotor, so the driving of the spherical rotor is not prevented by the increase of the friction force.

## 4.2. Experiment of rotational direction control

An experimental equipment shown in Fig. 4.3 is used to control the rotational direction of spherical ultrasonic motor using wire stators in order to investigate the effectiveness of PWM control. The spherical ultrasonic motor using wire stators is composed of one spherical rotor, four wire stators with waveguides and ultrasonic vibration sources. The Langevin transducer with resonance frequency of 24.6 kHz is used as an ultrasonic vibration source. Here, in order to control the rotational direction from No. 1 (Right) to No. 2 (Upper right) in Table 4.1, the vertical wire stator is connected with a vibration source, and the horizontal wire stators are connected with two vibration sources. In addition, the vibration sources are allocated by the alphabet from A to F. The vibration sources from A to D are connected to the outside waveguide of the wire stator, and the vibration sources of E and F are connected to the inside waveguide of the wire stator.

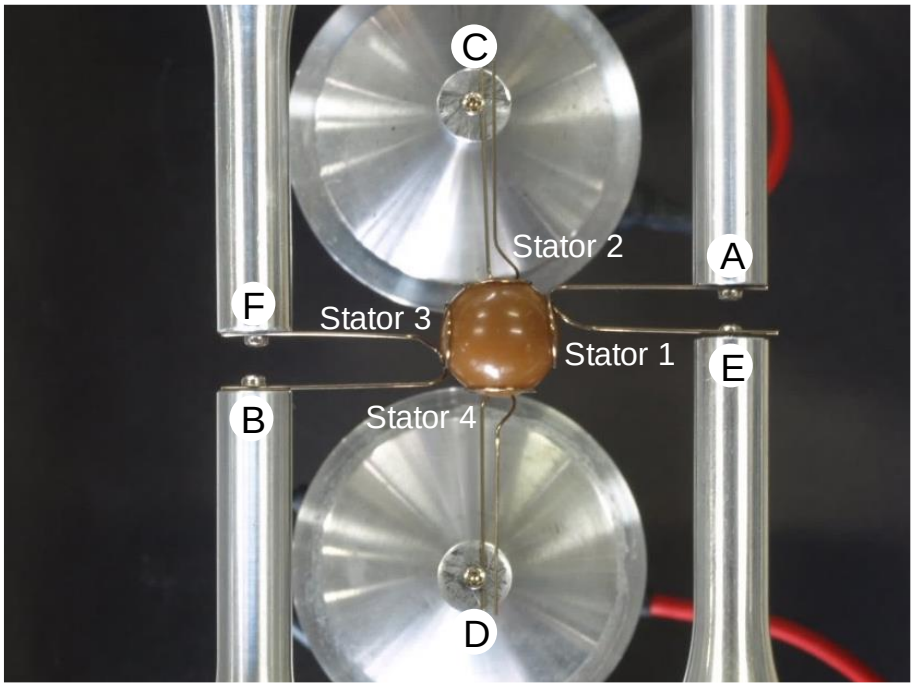


Fig. 4.3 Experimental equipment of PWM control experiment.

The output in forward rotation is synthesized so that the spherical rotor rotates upwards when the vibration sources from A to D are operated. The standing wave is generated in the horizontal wire stators and the vertical output is affected and the spherical rotor rotates in the right direction when all the vibration sources are operated from A to F. The horizontal output is regulated by the PWM control by the operation time of the vibration sources of E and F, and the spherical rotor rotates by changing the rotational direction between the upper right and the right. The vibration sources of E and F output respectively from the same waveform generator to synchronize the output timing.

The amplitude and frequency of the AC voltage applied to the vibration source are 20 $V_{p\text{-}p}$ and 24.6 kHz from A to F. The waveform generator used in the spherical ultrasonic motor using wire stators can adjust the generation time of AC voltage at a minimum of 0.001 s. In this study, an interval of 0.01 s is defined as a cycle. The duty ratio increases from 0% to 90% by 10% and the rotational angle is respectively measured. The spherical rotor with the reference point is used and the angle between the trajectory of the reference point and the horizontal direction is defined as the rotational angle.

## 4.3. Experimental results of rotational direction control

Experimental results are shown in Fig. 4.4. The rotational angle becomes smaller and smaller with the increase of the duty ratio. The influence of the horizontal wire stator output is reduced when the rotational angle is small. This result agrees with the initial idea that the horizontal wire stator output decreases with increasing the standing wave ratio. Therefore, the control method of the rotational direction using PWM control is effective.

The generation method of the standing wave can be considered as the cause of a sudden decrease in the rotational angle when the duty ratio is 50%. A waveform generator with 2 channel output is used. The output timing of the PWM control needs synchronization so that the same waveform generator is connected to E and F. Therefore, two traveling waves synthesized in the horizontal wire stators can be output from different waveform generators, and as a result the amplitude and frequency can be considered to be slightly different.

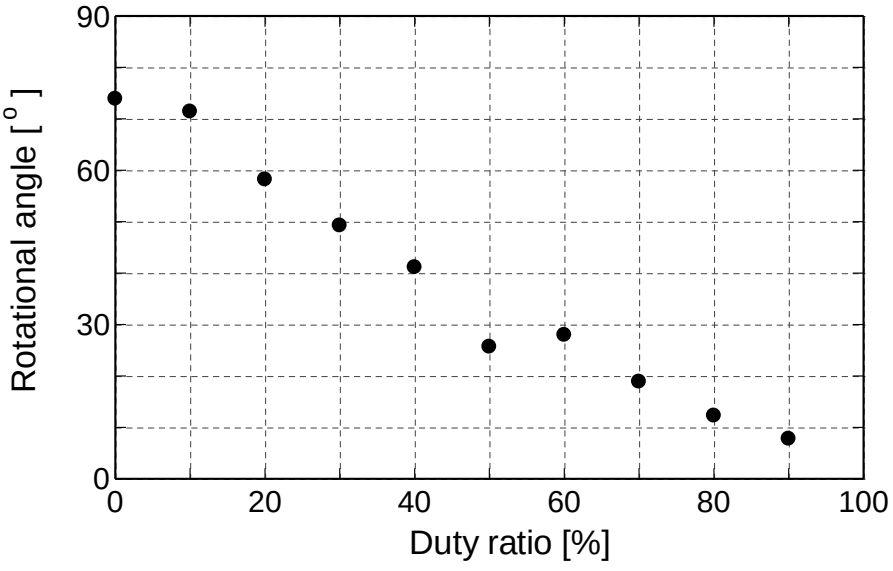


Fig. 4.4 Relationship between duty ratio and angle of rotational direction.

## 4.4. Summary of chapter 4

The rotational direction control of miniature spherical ultrasonic motor using wire stators is discussed. A PWM control method is proposed. The verification is carried out by the direction control experiment, and it can be shown that the proposed method is effective for the rotational direction control of miniature spherical ultrasonic motor using wire stators.

# Chapter 5. Evaluation on waveguide of stator

In this chapter, for the quantitative evaluation of the damping of the input vibration for the wire stator with the waveguide, the analysis by the finite element method for the wire stator is described. In this study, Femap with NX Nastran version 11.3.1 is used for the finite element analysis.

## 5.1. Damping evaluation of vibration by length of waveguide

The length of the coronary angioscopic catheter assumed as a requirement specification is approximately 2 m, whereas the wire stator used in the experiment up to the previous chapter has a waveguide30 mm which transmits vibration. Assuming the introduction of a coronary angioscopy, the wire stator with the waveguide extended to 2 m shown in Fig. 5.1 is designed. This is the 20 times model of the same scale as the wire stator used in the experiment. The size of the 20 times model with the one used in the experiments up to the previous chapter are shown in Table 5.1. The transient response analysis is performed by the finite element method in order to investigate the damping of vibration applied to this wire stator. The model used for finite element analysis is shown in Fig. 5.2. In addition, for comparison, a finite element model of the wire stator used in the experiment as shown in Fig. 5.3 is also made. In this model the transient response analysis is performed under the same conditions as that of the waveguide of 2 m.

As the material constant of each element, stainless steel SUS304 used in the 20 times model used in the experiment is applied. The values are shown in Table 5.2. Furthermore, the damping constant is obtained from the specific damping capacity (logarithmic decrement) $\delta = 0.01$ [42] (Fig. 5.4) of the material stainless steel. The relationship holds between $\delta$ and the damping constant $\xi$:

$$\delta = 2\pi\xi \Big/ \sqrt{1-\xi^2} \tag{5.1}$$ [43]

By transforming equation (5.1), the equation for obtaining $\xi$ from $\delta$ is obtained as follows:

$$\xi = \delta \Big/ \sqrt{4\pi^2 + \delta^2} \tag{5.2}$$

The value obtained by equation (5.2) is 0.15915%, and this value is input and the analysis is performed.

In this finite element analysis, the case where the Langevin transducer is connected to one end of a wire stator and ultrasonic vibration is input is reproduced. The vibration of the Langevin transducer depends on the waveform of the AC voltage, so the input waveform is a sine wave. The frequency of the sine wave is the resonance frequency of the Langevin transducer and the amplitude is referred to the amplitude of 40 $V_{p\text{-}p}$ AC voltage applied to the Langevin transducer used in the experiment. In addition, the analysis time can be assumed to be the time $\Delta T = 1/8f$ obtained by dividing one cycle $T = 1/f$ of each vibration load into eight. The analysis period is 1000 cycles, so the analysis time $T_a$ is expressed by the following equation.

$$T_a = \frac{1000}{f} \text{ [sec]} \tag{5.3}$$

From the above, the displacement input which reproduces the input vibration of the Langevin transducer is shown in Table 5.3. This input is made to the node of one end of the wire stator, and the displacement of the node of the coil part which is a contact part with the spherical rotor is output.

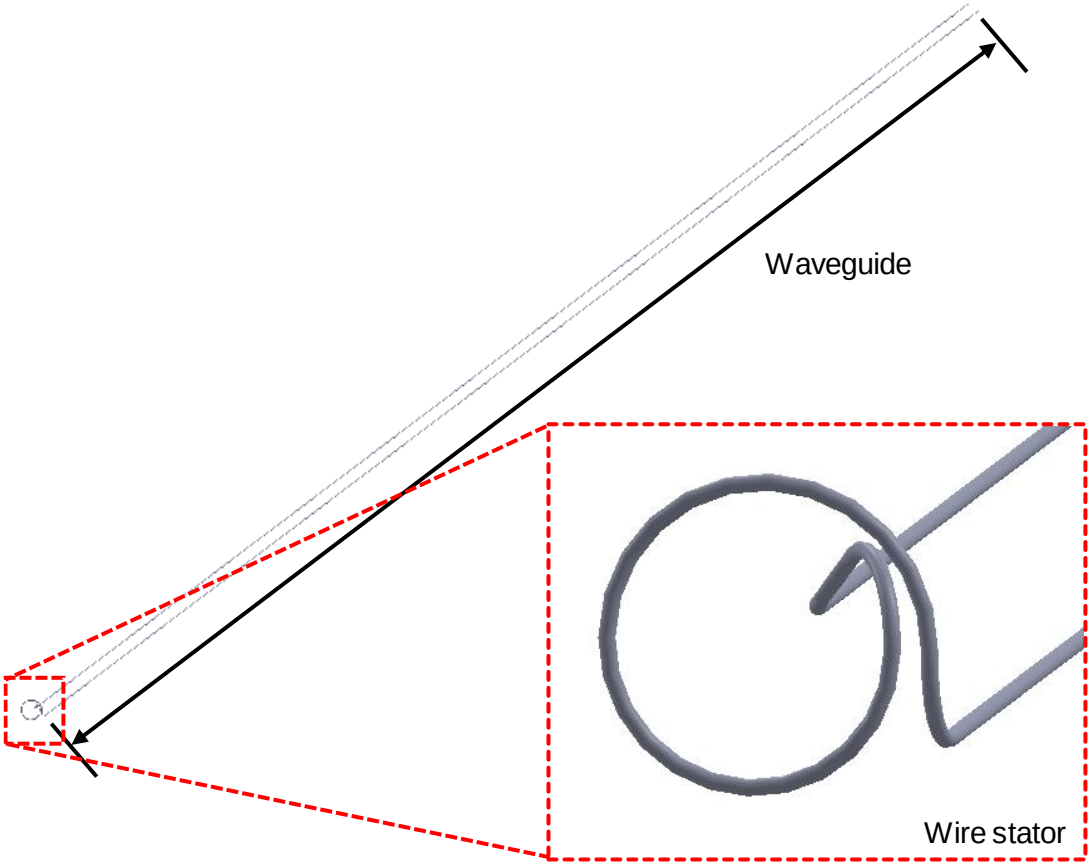


Fig. 5.1 Wire stator with long wave guide.

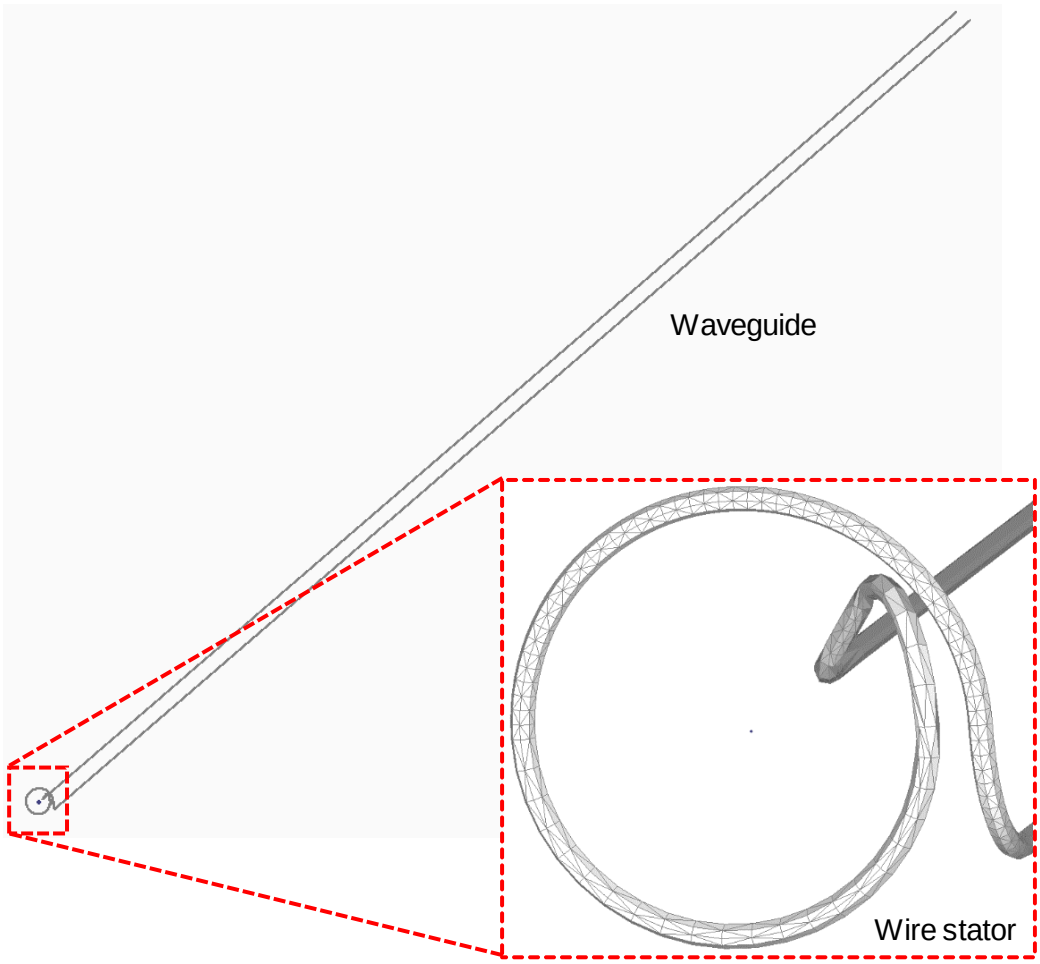


Fig. 5.2 Analysis model of wire stator with long wave guide.

Table 5.1 Size of wire stator and waveguide.

| | Experiment model | Long waveguide model |
|---|---|---|
| Length of waveguide [mm] | 30 | 2000 |
| Outside diameter of stator [mm] | 10 | |
| Wire diameter [mm] | 0.5 | |

Table 5.2 Material constant of SUS304.

| Young's modulus [GPa] | Poisson's ratio [-] | Density [kg/m$^3$] |
|---|---|---|
| 197 | 0.3 | 7930 |

Table 5.3 Simulation conditions.

| | |
|---|---|
| Input waveform [-] | Sine pulse |
| Frequency [kHz] | 24.6 |
| Amplitude [m] | 0.01 |
| Simulation time [s] | 0.0051 |
| Sampling time [s] | $5.0813\times10^{-6}$ |

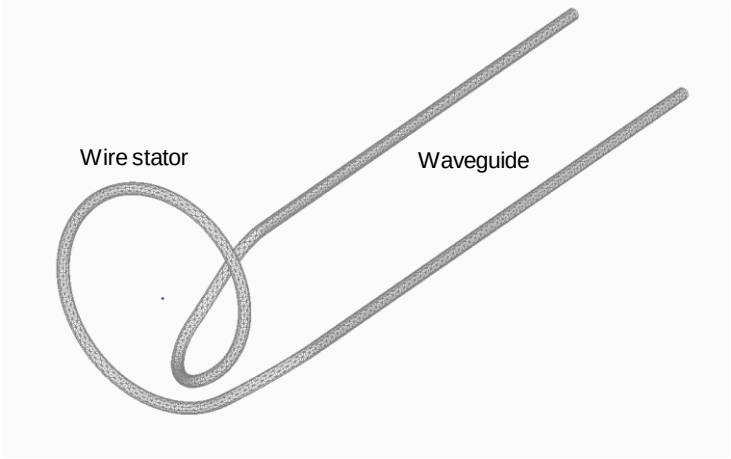


Fig. 5.3 Analysis model of wire stator of experiment type.

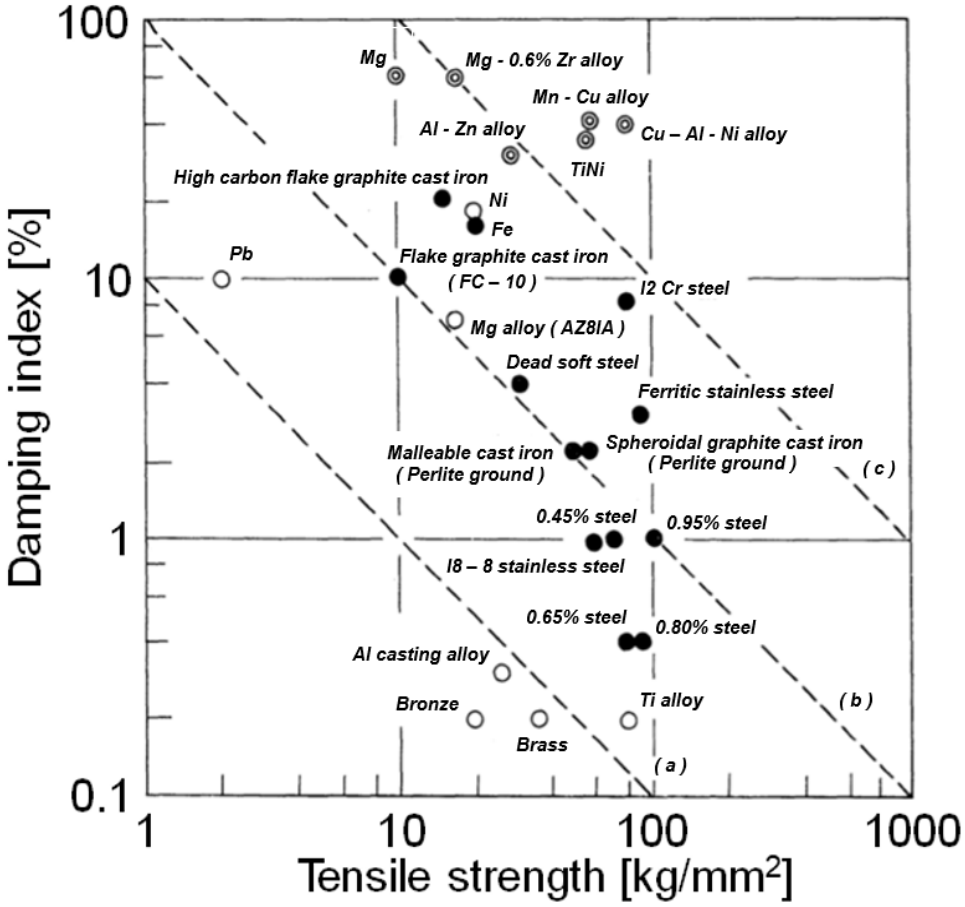


Fig. 5.4 Logarithmic decrement [42].

## 5.2. Evaluation of vibration by finite element method

The displacement from 0.0025 s to 0.003 s in the coil part of each stator obtained by analysis is shown in Fig. 5.5. It can be seen that the amplitude of the coil part of the long waveguide is clearly decreased as compared with the case where the waveguide is short. The amplitude of the stator with the 2000 mm waveguide is 0.026 mm and the amplitude of the stator with the 30 mm waveguide is 0.081 mm, which is decreased by 68.4%. In the previous study, the driving characteristic is evaluated by changing the voltage applied to the Langevin transducer which is the vibration source. At that time, the displacement due to the vibration of the tip of the Langevin transducer is measured with a laser displacement meter. As a result, it can be seen that, the amplitude of the displacement input to the coil stator increases as the applied voltage increases in the range of 60 $V_{p\text{-}p}$ or less. The decrease in input displacement at each voltage difference is shown in Fig. 5.6. From this figure, it can be seen that the decreasing rate of the amplitude is 68.4% which is obtained by extending the waveguide by approximately 67 times, and it almost agrees with the decreasing rate by decreasing the applied voltage by 30 $V_{p\text{-}p}$. From the above, it can be considered that the damping of vibration by extending the waveguide can be reproduced by changing the input of the Langevin transducer without using the same size experimental equipment.

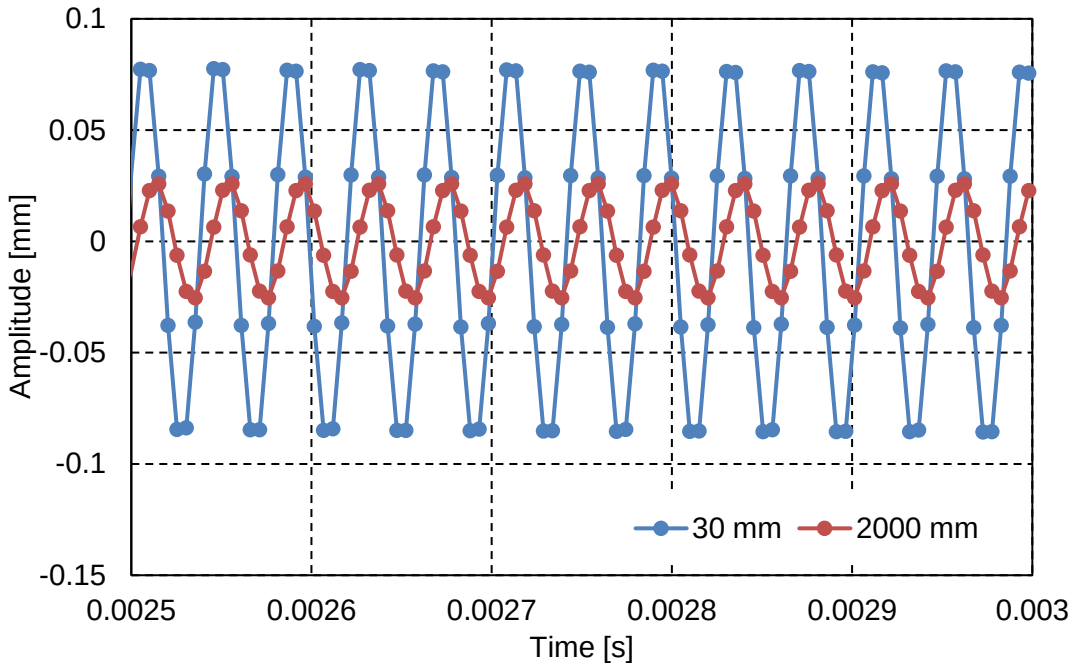


Fig. 5.5 Amplitude of wire stator.

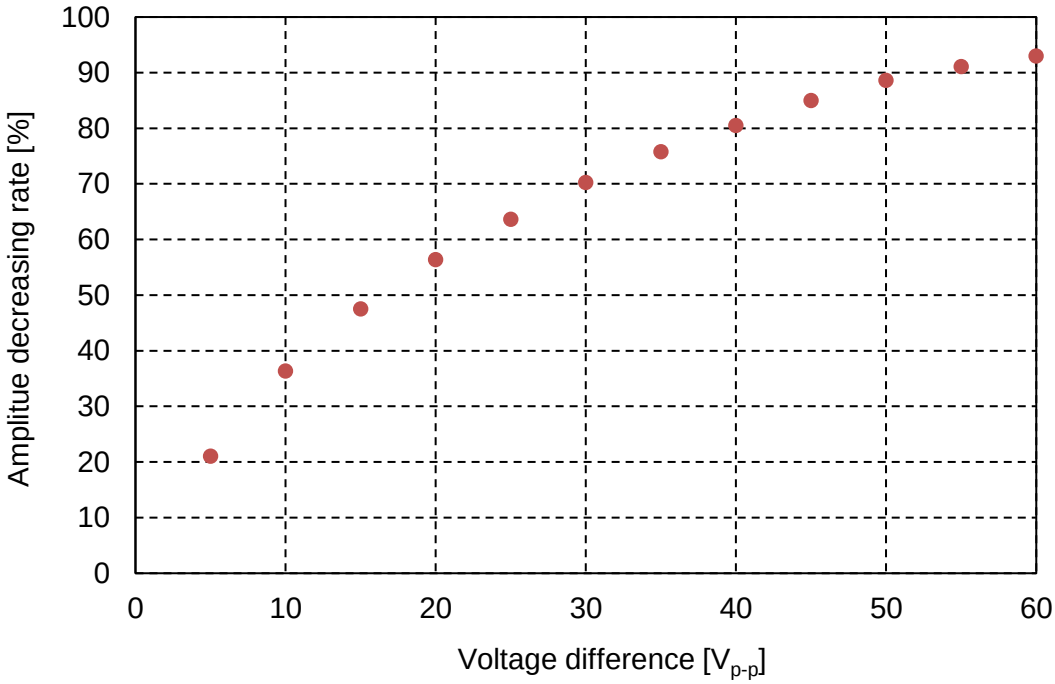


Fig. 5.6 Relationship between voltage difference and amplitude decreasing rate.

## 5.3. Validity of analysis result and influence of tube to damping

In addition, in order to verify the validity of the analysis result by the finite element method, the experiments for comparing the damping of vibration with 1 m wire and the analysis by the finite element method are performed (Fig. 5.7). The input AC voltage in the experiment is 40 $V_{p-p}$ and the frequency is 24.689 kHz which is the resonance frequency of the Langevin transducer. The initial value at the time of analysis is matched to the initial value in the experiment. The values of input amplitude and experimental amplitude are measured by the laser displacement meter (LK-G 5000 series, KEYENCE).

The amplitude value at the position of 1 m relative to the input amplitude of 0.022429 mm is 0.006737 mm in the experiment and 0.004871 mm at the time of analysis by the finite element method. A good agreement can be found between the experimental results and the analysis results by the finite element method. The spherical rotor can rotate if it has such amplitude damping.

In addition, it can be considered that the vibration is greatly attenuated by inserting the wire into the tube. Therefore, the damping of the vibration caused by the contact of the wire and the wall of the tube is investigated in the experiment by using 1 m tube with two different materials (ABS, stainless steel). The input AC voltage in the experiment is 40 $V_{p-p}$ and the frequency is 24.694 kHz which is the resonance frequency of the Langevin transducer.

The amplitude value at the position of 1 m relative to the input amplitude of 0.01819 mm and 0.01870 mm respectively after passing through the tube is 0.002283 mm when the material is ABS tube and 0.001844 mm when the material is stainless steel tube. The damping of the ABS tube is smaller than that of stainless steel, and the spherical rotor can rotate if it has such amplitude damping. As a supplement, the actual material of the catheter is silicon, polyurethane, polyethylene, Teflon, etc.

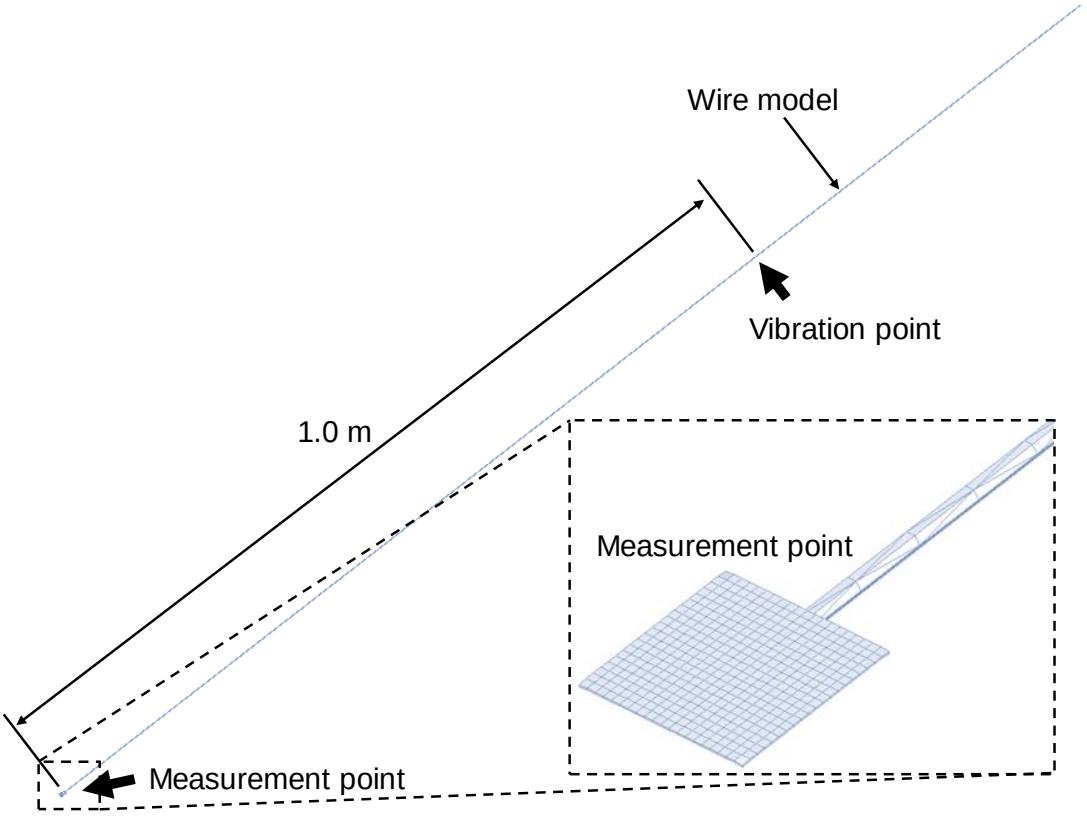


Fig. 5.7 Analysis model for comparing the damping of vibration.

## 5.4. Summary of chapter 5

Assuming the introduction of a coronary angioscopy, the wire stator with the waveguide of 2 m is designed. The transient response analysis by the finite element method is performed for this model and the model with the waveguide of 30 mm used in the experiment, and the decreasing rate of the input amplitude due to the influence of the waveguide can be clarified.

# Chapter 6. Evaluation on support part of stator

In this chapter, for the quantitative evaluation of the damping of the input vibration for the wire stator with the support part, the analysis by the finite element method for the wire stator is described. In this study, Femap with NX Nastran version 11.3.1 is used for the finite element analysis.

## 6.1. Damping evaluation of vibration in waveguide support model

As described in the previous chapter, assuming the introduction of a coronary angioscopic catheter, the length of the wire stator is approximately 2 m, so it is necessary to support the waveguide in operation. As shown in Fig. 6.1, a support structure is added to the model of the coil stator in this study, and a transient response analysis is performed by the finite element method. All the materials of the added structure are SUS304 which is the same as the material of the stator, and the line diameter of the rod part is the same as the stator. As the material constant, the values used for analysis are shown in Table 6.1.

Furthermore, the damping constant is obtained from the specific damping capacity (logarithmic decrement) $\delta$ = 0.01 [42] of the material stainless steel. The relationship holds between $\delta$ and the damping constant $\xi$:

$$\delta = 2\pi\xi \Big/ \sqrt{1-\xi^2} \qquad (6.1)\ [43]$$

By transforming equation (6.1), the equation for obtaining $\xi$ from $\delta$ is obtained as follows:

$$\xi = \delta \Big/ \sqrt{4\pi^2+\delta^2} \qquad (6.2)$$

The value obtained by equation (6.2) is 0.15915%, and this value is input and the analysis is performed.

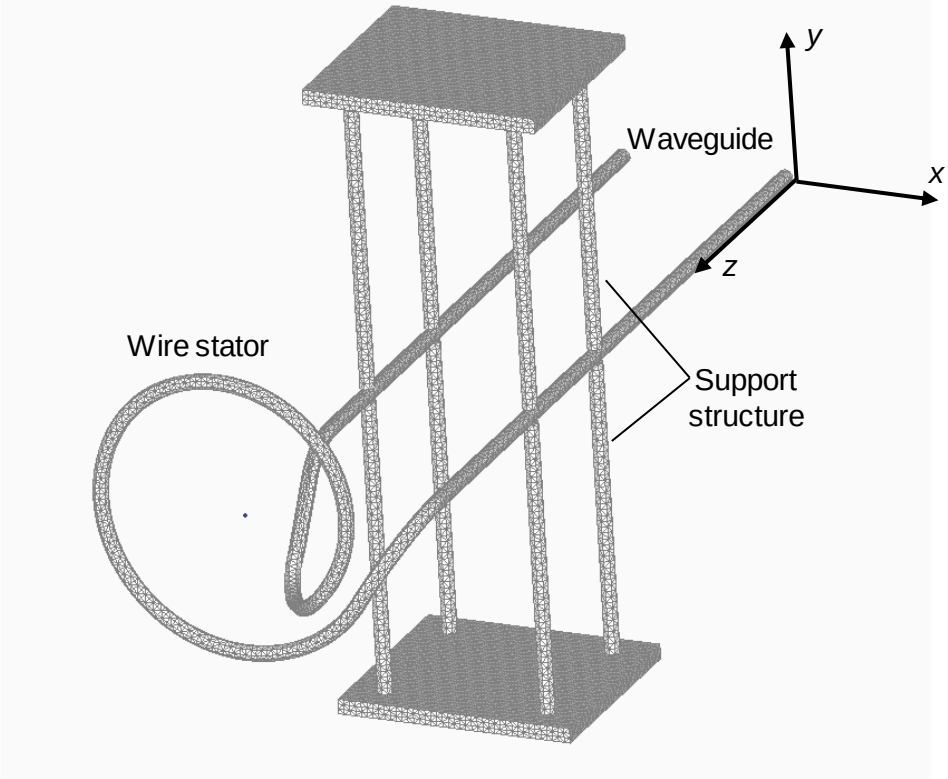


Fig. 6.1 Analysis model of wire stator with support.

Table 6.1 Material constant of SUS304.

| Young's modulus [GPa] | Poisson's ratio [-] | Density [kg/m$^3$] |
|---|---|---|
| 197 | 0.3 | 7930 |

In this finite element analysis, the case where the Langevin transducer is connected to one end of a wire stator and ultrasonic vibration is input is reproduced. The vibration of the Langevin transducer depends on the waveform of the AC voltage, so the input waveform is a sine wave. The frequency of the sine wave is the resonance frequency of the Langevin transducer and the amplitude is referred to the amplitude of 40 $V_{p\text{-}p}$ AC voltage applied to the Langevin transducer used in the experiment. In addition, the analysis time can be assumed to be the time $\Delta T = 1/8f$ obtained by dividing one cycle $T = 1/f$ of each vibration load into eight. The analysis period is 1000 cycles, so the analysis time $T_a$ is expressed by the following equation.

$$T_a = \frac{1000}{f} \text{ [sec]} \tag{6.3}$$

From the above, the displacement input which reproduces the input vibration of the Langevin transducer is shown in Table 6.2. This input is made to the node of one end of the wire stator.

The displacement of the node of the coil part which is the contact part with the spherical rotor is output. In the input, the direction perpendicular to the support rod is defined as $x$ direction, and the parallel direction is defined as $y$ direction, and the direction of the displacement in the node of the coil part output in these two directions is $z$ direction.

Table 6.2 Simulation conditions.

| Input waveform [-] | Sine pulse |
|---|---|
| Frequency [kHz] | 24.6 |
| Amplitude [m] | 0.01 |
| Simulation time [s] | 0.0051 |
| Sampling time [s] | $5.0813\times10^{-6}$ |

## 6.2. Evaluation of vibration by finite element method

The analysis results are from 0.0025 s to 0.003 s shown in Fig. 6.2 when the displacement input is made in *x* direction, and the analysis results from 0.0025 s to 0.003 s shown in Fig. 6.3 when the displacement input is made in *y* direction.

As shown in Fig. 6.2, the amplitude in the coil part of the stator having the support structure in the waveguide is 0.058 mm, and the amplitude in the coil part of the stator having no support structure in the waveguide is 0.081 mm. From this result, when the displacement input is made in the direction perpendicular to the support rod, it can be seen that the influence on the amplitude of the support appears as a decrease of 27.3%.

In addition, as shown in Fig. 6.3, the amplitude in the coil part of the stator having the support structure in the waveguide is 0.091 mm and the amplitude in the coil part of the stator having no support structure in the waveguide is 0.27 mm. From this result, when the displacement input is made in the direction parallel to the support rod, it can be seen that the influence on the amplitude of the support appears as a decrease of 66.8%. Comparing these two results, the amplitude is decreased by 39.5% when the displacement input is made in *y* direction rather than in *x* direction. As a reason of such a result, the vibration in the direction can hardly bend the support structure due to the structure and it can be considered that the amplitude is suppressed by the support structure. From the above, it can be confirmed that the vibration transmitted to the coil part varies depending on the direction of the displacement input made to the tip with the same support structure. In addition, it can be considered that the traveling wave close to parallel to the support structure attenuates.

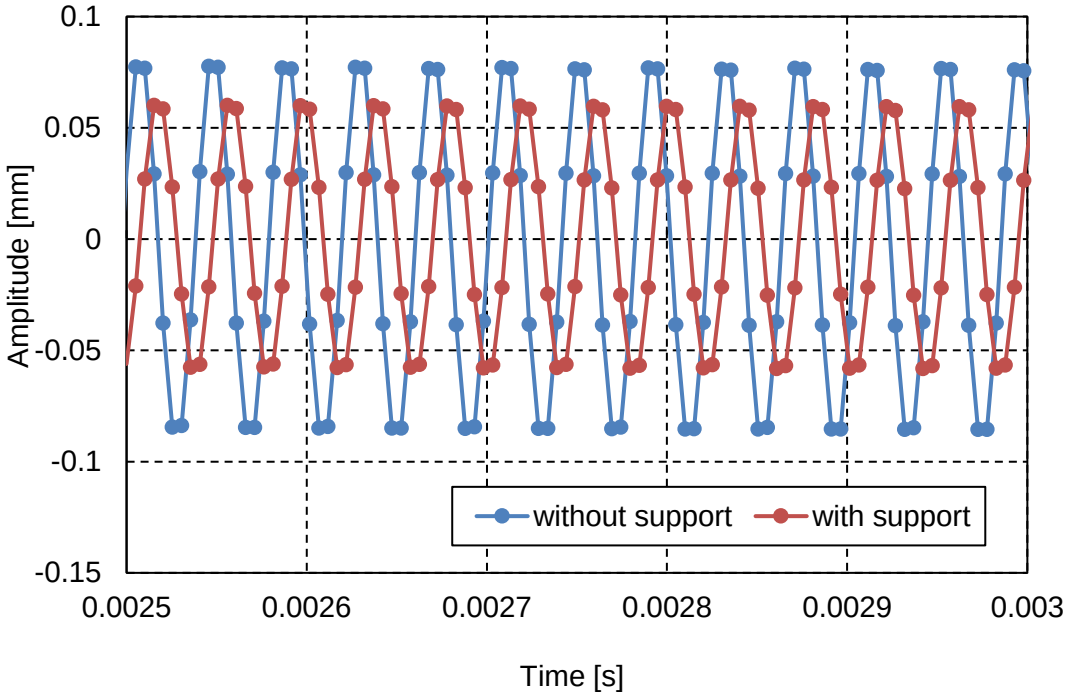


Fig. 6.2 Amplitude of wire stator (input of x direction).

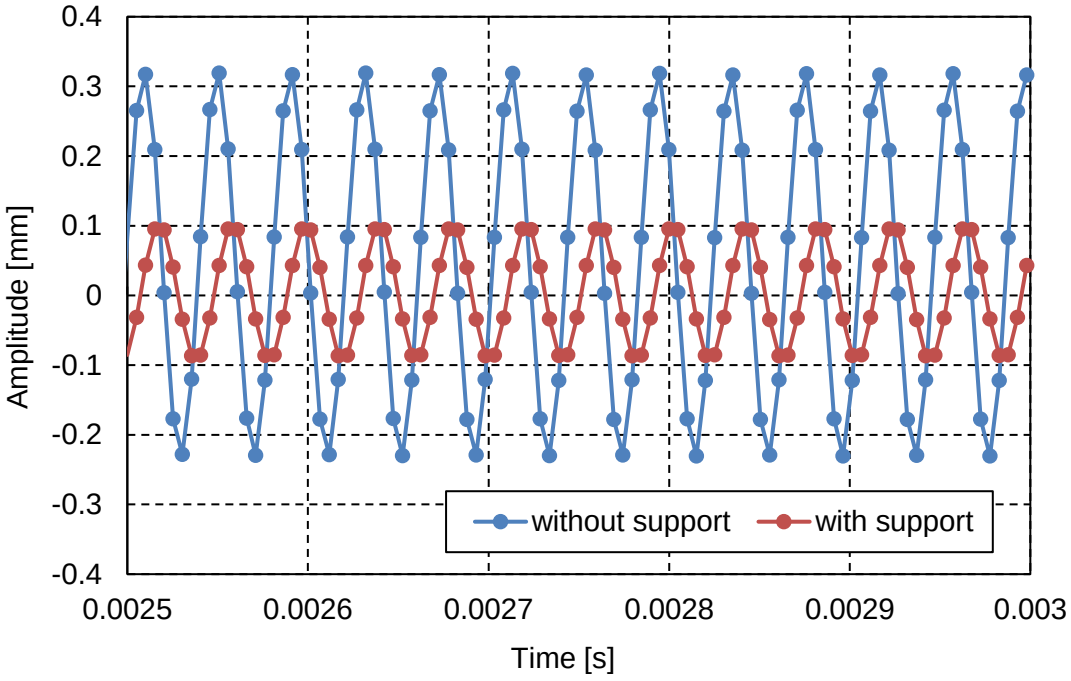


Fig. 6.3 Amplitude of wire stator (input of y direction).

## 6.3. Improvement of waveguide support model and evaluation by finite element method

It can be seen that the added support structure greatly decreases the amplitude in *y* direction with a large output in section 6.2. Based on the result, a structure which can hardly inhibit the amplitude in *y* direction is devised. The model with an improved support structure is shown in Fig. 6.4. In section 6.2, it can be considered that the vibration in the direction perpendicular to the pillar part of the support structure can be hardly attenuated, so the support structure is added from the direction perpendicular to *y* direction, that is from *x* direction. In addition, in order to arrange the conditions other than the support direction, the model in which a pillar is partially removed from the initial model support structure is made. This is the model with the support structure add from *y* direction. The model is shown in Fig. 6.5. The displacement input is performed under the conditions shown in Table 6.2 for these two models, and a transient response analysis is performed with the input direction as *y* direction.

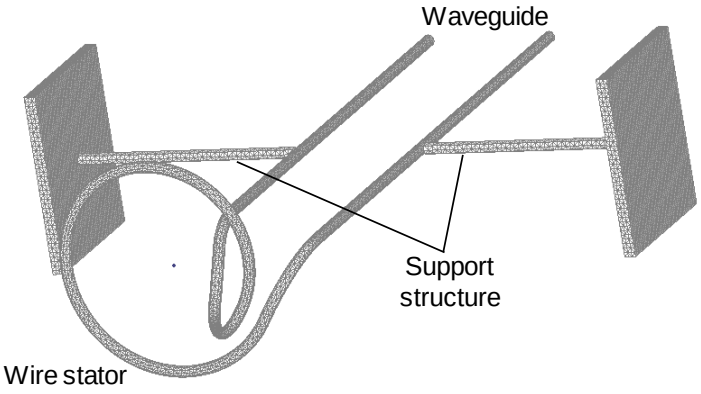


Fig. 6.4 Improved wire stator model (x direction support).

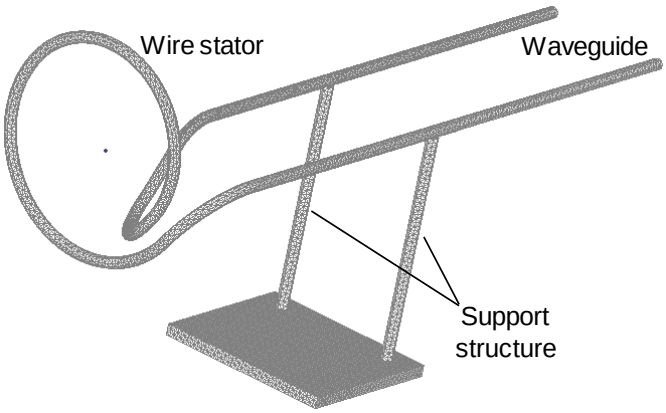


Fig. 6.5 Improved wire stator model (y direction support).

## 6.4. Damping evaluation results by finite element method of improved model

In the two models, the analysis results are from 0.0025 s to 0.003 s shown in Fig. 6.6 when the displacement input is made in *y* direction. In the improved fixing method, there is almost no great difference in the damping amount due to the difference in support direction as shown in Fig. 6.6. From this result, it can be considered that the difference in the amplitude damping by the displacement input direction in section 6.2 is not due to the influence of the support direction, but due to the rigidity of the entire structure. The analysis results of the improved *x* direction support models and the model without the support structure are shown in Fig 6.7. The amplitude at the coil part of the stator with no support structure in the waveguide is 0.27 mm, and the amplitude at the coil part of the *x* direction support model is 0.25 mm. From this result, it can be clarified that the decreasing rate of the amplitude is 8.6% and the amplitude damping can be greatly reduced than before the improvement when the improved support structure is added to the wire stator. From the above, it can be considered that the improved support structure is a structure which can hardly inhibit ultrasonic vibration, so it can be said that it is more suitable support structure.

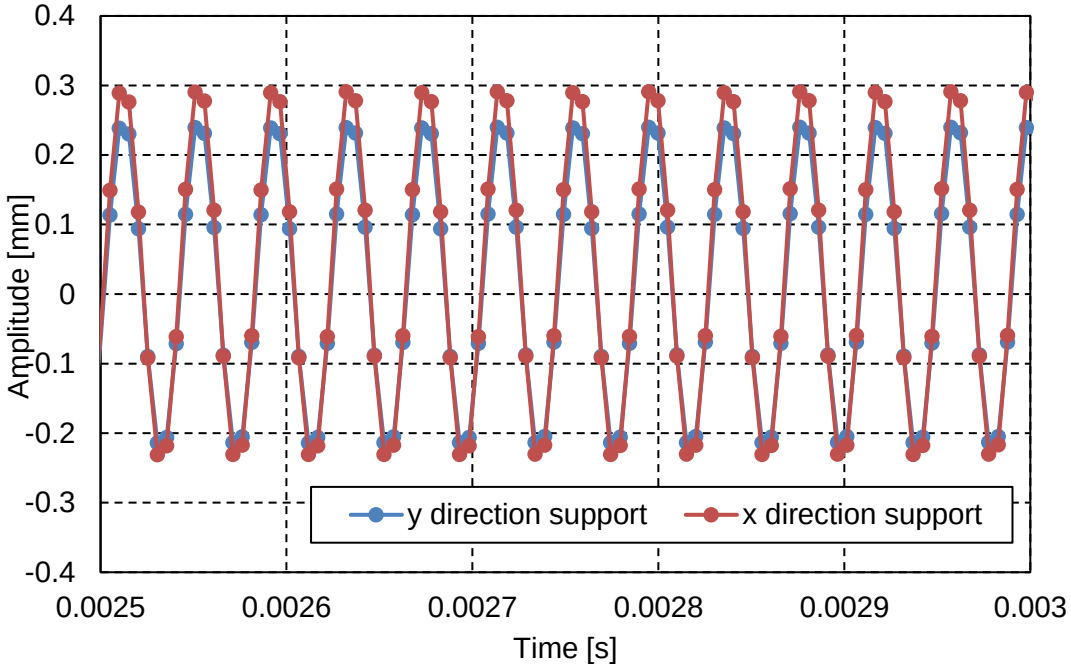


Fig. 6.6 Amplitude of wire stator (difference of support direction).

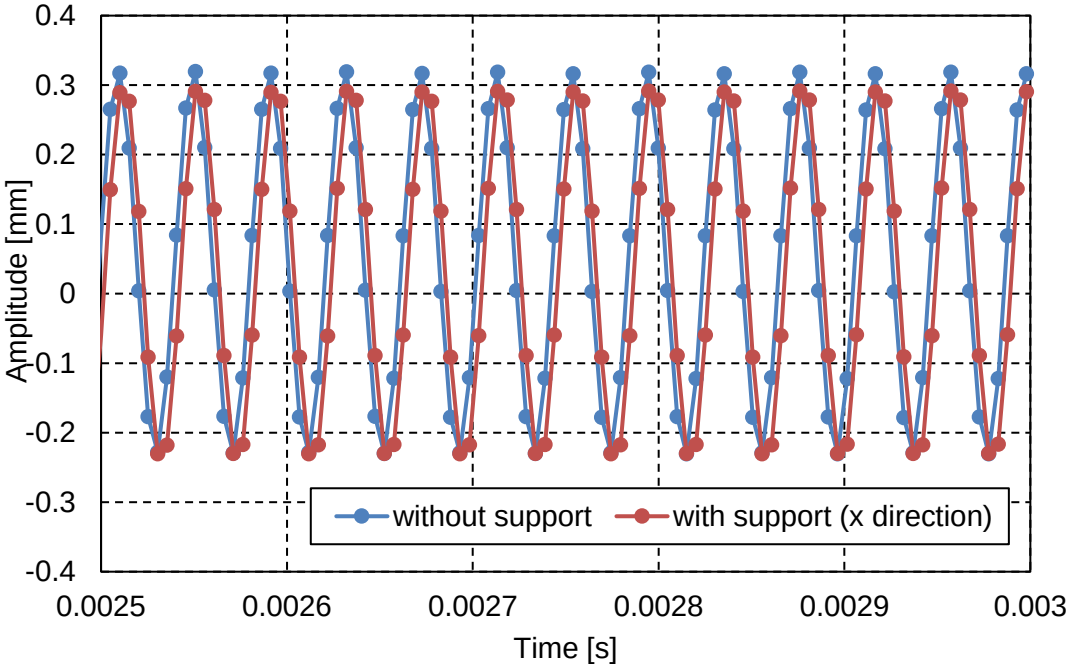


Fig. 6.7 Amplitude of wire stator (with and without support structure).

## 6.5. Summary of chapter 6

The transient response is performed by the finite element method for the model of the wire stator with the support structure added, and the influence of damping by the structure and the vibration direction can be clarified. In addition, based on this, a more appropriate support structure is devised, and the damping of the input vibration can be effectively reduced by performing the transient response analysis.

# Chapter 7. Conclusions

## 7.1. Summary

In this study, the development of a miniature spherical ultrasonic motor for direction control of a Coronary angiographic camera is attempted. A miniature spherical ultrasonic motor using wire stators composed of a spherical rotor, a wire stator, a waveguide and a vibration source is made. The wire stator is a spiral type stator of one spiral and has two waveguides on the outside and inside.

First, the pressing force of ultrasonic motor which is an important factor in developing an ultrasonic motor is investigated. The relationship between the pressing force and the rotational number is investigated, and it can be clarified that there is an optimum value for the pressing force and there is the difference between the forward rotation and the reverse rotation.

Next, the starting torque which is one characteristic of the motor is investigated. The relationship between the frequency and the amplitude of the applying AC voltage and the starting torque is investigated, and it can be clarified that there is a difference between the forward rotation and the reverse rotation.

Next, the rotational direction control of this motor is discussed. The application method of PWM control as the control method is proposed. The verification is carried out by the direction control experiment, and it can be shown that the proposed method is effective for the rotational direction control of a miniature spherical ultrasonic motor using wire stators. By the direction control experiment, it can be shown that the proposed method is effective for the rotational direction control of a miniature spherical ultrasonic motor using wire stators.

Finally, for the quantitative evaluation of the damping of input vibration for a wire stator, the analysis by the finite element method for the wire stator is performed. Assuming the introduction of a coronary angioscopy, the wire stator with the waveguide of 2 m is designed. The transient response analysis by the finite element method is performed for this model and the model with the waveguide of 30 mm used in the experiment, and the decreasing rate of the input amplitude due to the influence of the waveguide can be clarified. In addition, the transient response is performed by the finite element method for the model of the wire stator with the support structure added, and the influence of damping by the structure and the vibration direction can be clarified. In addition, based on this, a more appropriate support structure is devised, and the damping

of the input vibration can be effectively reduced by performing the transient response analysis.

# References

[1] Ministry of Health, Labour and Welfare, “Annual Health, Labour and Welfare Report 2017 - General Welfare and Labour -”, MHLW NET, https://www.mhlw.go.jp/english/wp/wp-hw11/dl/01e.pdf (2018, November 3).

[2] Yock, P.G., Linker, D.T., and Angelsen, B.A., “Two-dimensional intravascular ultrasound: technical development and initial clinical experience”, Journal of the American Society of Echocardiography, Vol. 2, No. 4 (1989), pp. 296-304.

[3] Mintz, G.S., Nissen, S.E., Anderson, W.D., Bailey, S.R., Erbel, R., Fitzgerald, P.J., Pinto, F.J., Rosenfield, K., Siegel, R.J., Tuzcu, E.M., and Yock, P.G., “American College of Cardiology clinical expert consensus document on standards for acquisition, measurement and reporting of intravascular ultrasound studies (IVUS). A report of the American College of Cardiology task force on clinical expert consensus documents developed in collaboration with the European Society of Cardiology endorsed by the society of cardiac angiography and interventions”, Journal of the American College of Cardiology, Vol. 37, No. 5 (2001), pp. 1478-1492.

[4] Mizuno, K., Miyamoto, A., Isojima, K., Kurita, A., Senoo, A., Arai, T., Kikuchi, M., and Nakamura, H., “A serial observation of coronary thrombi in vivo by a new percutaneous transluminal coronary angioscope”, Angiology, Vol. 43, No. 2 (1992), pp. 91-99.

[5] Thieme, T., Wernecke, K.D., Meyer, R., Brandenstein, E., Habedank, D., Hinz, A., Felix, S.B., Baumann, G., and Kleber, F.X., “Angioscopic evaluation of atherosclerotic plaques: validation by histomorphologic analysis and association with stable and unstable coronary syndromes”, Journal of the American College of Cardiology, Vol. 28, No. 1 (1996), pp. 1-6.

[6] Uchida, Y., Tomaru, T., Nakamura, F., Furuse, A., Fujimori, Y., and Hasegawa, K., “Percutaneous coronary angioscopy in patients with ischemic heart disease”, American Heart Journal, Vol. 114, Issue 5 (1987), pp. 1216-1222.

[7] Uchida, Y., Hasegawa, K., Kawamura, K., and Shibuya, I., “Angioscopic observation of the coronary luminal changes induced by percutaneous transluminal coronary angioplasty”, American Heart Journal, Vol. 117, Issue 4 (1989), pp. 769-776.

[8] Spears, J.R., Marais, H.J., Serur, J., Pomerantzeff, O., Geyer, R.P., Sipzener, R.S., Weintraub, R., Thurer, R., Paulin, S., Gerstin, R., and Grossman, W., “In vivo coronary angioscopy”, Journal of the American College of Cardiology, Vol. 1, No. 5 (1983), pp. 1311-1314.

[9] Sherman, C.T., Litvack, F., Grundfest, W., Lee, M., Hickey, A., Chaux, A., Kass, R., Blanche, C., Matloff, J., Morgenstern, L., Ganz, W., Swan, H.J.C., and Forrester, J., “Coronary angioscopy in patients with unstable angina pectoris”, The New England Journal of Medicine, Vol. 315, No. 15 (1986), pp. 913-919.

[10] Cribier, A., Jolly, N., Eltchaninoff, H., Koning, R., Baala, B., Kothari, M., Chan, C., and Letac, B., “Angioscopic evaluation of prolonged vs standard balloon inflations during coronary angioplasty: A randomized study”, European Heart Journal, Vol. 16, Issue 7 (1995), pp. 930-935.

[11] Siegel, R.J., Ariani, M., Fishbein, M.C., Chae, J.S., Park, J.C., Maurer, G., and Forrester, J.S., “Histopathologic validation of angioscopy and intravascular ultrasound”, Circulation, Vol. 84, No. 1 (1991), pp. 109-117.

[12] Mizuno, K., Arai, T., Satomura, K., Shibuya, T., Arakawa, K., Okamoto, Y., Miyamoto, A., Kurita, A., Kikuchi, M., Nakamura, H., Utsumi, A., and Takeuchi, K., “New percutaneous transluminal coronary angioscope”, Journal of the American College of Cardiology, Vol. 13, No. 2 (1989), pp. 363-368.

[13] White, C.J., Ramee, S.R., Collins, T.J., Mesa, J.E., and Jain, A. “Percutaneous angioscopy of saphenous vein coronary bypass grafts”, Journal of the American College of Cardiology, Vol. 21, No. 5 (1993), pp. 1181-1185.

[14] White, C.J., Ramee, S.R., Collins, T.J., Jain, S.P., and Escobar, A., “Cornary angioscopy of abrupt occlusion after angioplasty”, Journal of the American College of Cardiology, Vol. 25, No. 7 (1995), pp. 1681-1684.

[15] Shikata, H., Kobata, T., Hida, K., Noguchi, Y., Kiyosawa, J., Sakamoto, S., and Matsubara, J., “Endovascular revascularization under carbon dioxide angiography”, Japanese Journal of Cardiovascular Surgery, Vol. 34, No. 4 (2005), pp. 237-242.

[16] Honye, J. and Saito, S., IVUS manual, (2006), Nakayama-Shoten [published in Japanese].

[17] Hayashi, A., Tsuboi, M., Ikeda, N., Kajiwara, N., Yoshida, K., Ichinose, S., Nagata S., Kono, T., Okunaka, T., Hirano, T., and Kato, H., “Development and future of the convex scanning type Ultrasonic Bronchofiberscope and Optical Coherence Tomography”, the Journal of the Japan Society for Bronchology, Vol. 25, No. 8 (2003), pp. 595-602.

[18] Ikejima, H., Kitabata, H., and Akasaka, T, “Current status and future perspectives of coronary artery imaging by optical coherence tomography”, Journal of the Japanese Coronary Association, Vol. 16, No. 1 (2010), pp. 73-79.

[19] Okamatsu, K., Seino, Y., and Mizuno, K., “Novel Coronary Imaging Insight into the Acute Coronary Syndromes from Angioscopic Studies (II)”, Japanese Journal of the Medical Association of Nippon Medical School, Vol. 5, Issue 1 (2009), pp. 6-8.

[20] Uchida, Y., “Cardioangioscopy”, (1995), MEDICAL VIEW [published in Japanese].

[21] Uchida, Y., Fujimori, Y., Tomaru, T., Oshima, T., and Hirose J, “Percutaneous angioplasty of chronic obstruction of peripheral arteries by a temperature-controlled Nd:YAG laser system”, Journal of Interventional Cardiology, Vol. 5, Issue 4 (1992), pp. 301-308.

[22] Toyama, S., Sugitani, S., Zhang, G., Miyatani, Y., and Nakamura, K., “Multi degree of freedom spherical ultrasonic motor”, Proceedings of IEEE International Conference on Robotics and Automation, (1995), pp. 2935-2940.

[23] Sashida, T. and Kenjo, T., An Introduction to Ultrasonic Motors (1993), Oxford University Press.

[24] Kamata, M., “Development of micro spherical ultrasonic motor for endoscopic

camera", M.S. thesis, Department of Mechanical Systems Engineering, Tokyo University of Agriculture and Technology, Tokyo, Japan, 2012 [published in Japanese].

[25] Sashida, T., "Trial construction and operation of an ultrasonic vibration driven motor -Theoretical and experimental investigation of its performances-", OYO BUTURI, Vol. 51, No. 6 (1982), pp. 713-720 [published in Japanese].

[26] Hagedorn, P. and Wallaschek, J., "Travelling wave ultrasonic motors, Part I: Working principle and mathematical modelling of the stator", Journal of Sound and Vibration, Vol. 155, No. 1 (1992), pp. 31-46.

[27] Hagedorn, P. and Wallaschek, J., "Travelling wave ultrasonic motors, Part II: Numerical Method for the flexural vibrations of the stator", Journal of Sound and Vibration, Vol. 168, No. 1 (1993), pp. 115-122.

[28] Moal, P.L.E. and Minotti, P., "A 2-D analytical approach of the stator-rotor contact problem including rotor bending effects for high torque piezomotor design", European Journal of Mechanics - A/Solids, Vol. 16, No. 6 (1997), pp. 1067-1103.

[29] Wallaschek, J., "Contact mechanics of piezoelectric ultrasonic motors", Smart Materials and Structures, Vol. 7, No. 3 (1998), pp. 369-381.

[30] Kandare, G. and Wallaschek, J., "Derivation and validation of a mathematical model for traveling wave ultrasonic motors", Smart Materials and Structures, Vol. 11, No. 4 (2002), pp. 565-574.

[31] Zhao, C., "Some proposals for development of ultrasonic motor techniques in China", Micromotors Servo Technique, Vol. 39, No. 2 (2006), pp. 64-67 [published in Chinese].

[32] Bekiroglu E., "Ultrasonic motors: Their models, drives, controls and applications", Journal of Electroceramics, Vol. 20, No. 3-4 (2008), pp. 277-286.

[33] Kenjou, T. and Sashida, T., Ultrasonic motor guide, (1991), Sogo-denshi [published in Japanese].

[34] Kawachi, K., Ultrasonic motor / Actuator, (1986), Triceps [published in Japanese].

[35] Maeno, T., “Ultrasonic motors”, Journal of the Robot Society of Japan, Vol. 21, No. 1 (2003), pp. 10-14.

[36] Kaga, T., “Development of ultrasonic motor with coil type stator and its application to vascular endoscope”, M.S. thesis, Department of Mechanical Systems Engineering, Tokyo University of Agriculture and Technology, Tokyo, Japan, 2009 [published in Japanese].

[37] Sawanobori, T., Akiyama, Y., and Nakamura, M., “Effects of Pitch Angle and Damping on Stresses in Helical Spring”, Transactions of the Japan Society of Mechanical Engineers Series C, Vol. 52, No. 473 (1986), pp. 154-162.

[38] Yano, T. and Maeno, T., “Spherical motor”, Journal of the Robot Society of Japan, Vol. 21, No. 7 (2003), pp. 740-743.

[39] Miyoshi, O., “Optimum design of stator for the spherical ultrasonic motor”, M.S. thesis, Department of Mechanical Systems Engineering, Tokyo University of Agriculture and Technology, Tokyo, Japan, 1997 [published in Japanese].

[40] Wang, F., Nishizawa, U., and Toyama, S., “Multi degree-of-freedom micro spherical ultrasonic motor using wire stators”, Vibroengineering PROCEDIA, Vol. 10, (2016), pp. 272-276.

[41] Wang, F., Nishizawa, U., and Toyama, S., “Micro spherical ultrasonic motor using single spiral wire stators”, Vibroengineering PROCEDIA, Vol. 13, (2017), pp. 121-126.

[42] Sugimoto, K., “High-damping alloys - A review on basic problem and application -”, Vol. 14, No. 7 (1975), pp. 491-498.

[43] Kishi, M., Finite element method practice handbook, (2006), Morikita [published in Japanese].

# Thanks

When summarizing this paper, please accept my heartfelt thanks to teacher Shigeki Toyama, Professor of the Division of Advanced Mechanical Systems Engineering at Institute of Engineering, Graduate Schools, Tokyo University of Agriculture and Technology for his always sincere and patient guidance.

In addition, please accept my sincere thanks to teachers, Vice Chair of the Division of Advanced Mechanical Systems Engineering at Institute of Engineering, Graduate Schools, Tokyo University of Agriculture and Technology for their useful advices for this study.

Please accept my sincere thanks to teacher Uichi Nishizawa, Assistant Professor of the Division of Advanced Mechanical Systems Engineering at Institute of Engineering, Graduate Schools, Tokyo University of Agriculture and Technology for his not only research but also various support.

When summarizing this paper, please accept my sincere thanks to Mr. Hideki Tanaka in grade 2 of Master Course in the Toyama laboratory for his help.

Please accept my sincere thanks to Mr. Kota Suzuki and Mr. Yuto Sawama, OB in the Toyama laboratory, Dr. Taro Oohashi in Doctoral Course, OB in the Toyama laboratory and Mr. Toshitake Araie and Mr. Soji Shimono in Doctoral Course in the Toyama laboratory for their helps. Please accept my sincere thanks to everyone in the Toyama laboratory for their various guidance.

Please accept my sincere thanks to Ms. Keiko Nakayama, Secretary in the Toyama laboratory for her cooperation about administrative relations. In addition, please accept my sincere thanks to the students, OB in the Toyama laboratory at the Tokyo University of Agriculture and Technology for their research guidance in my Doctoral study life.

Fulin Wang
February 2019